J. Fluid Mech. (1987), *vol.* 182, *pp.* 47–83
Printed in Great Britain

A turbulent flow over a curved hill
Part 1. Growth of an internal boundary layer

By V. BASKARAN,† A. J. SMITS‡ AND P. N. JOUBERT
Department of Mechanical Engineering, University of Melbourne, Parkville 3052, Australia

(Received 18 February 1985 and in revised form 15 January 1987)

Two experiments were performed to study the response of turbulent boundary layers to sudden changes in surface curvature and pressure gradient. In the first experiment, the behaviour of a boundary layer negotiating a two-dimensional curved hill was examined. Prior to separating on the leeward side of the hill, the layer experienced a short region of concave surface curvature, followed by a prolonged region of convex surface curvature. The corresponding pressure gradient changed from adverse to favourable, and back to adverse. In the second experiment, the flow over a symmetrical wing was studied. This wing had the same profile as the hill with a very similar pressure distribution. The obvious difference between the two experiments was the use of leading and trailing edge plates in the hill flow. The results show that an internal layer forms in the flow over the curved hill, and that this internal layer displays many similarities to the boundary layer observed on the free wing. The internal layer grows as an independent boundary layer beneath a turbulent free-shear layer, and as it develops it establishes its own wall (inner) and wake (outer) regions. The perturbation responsible for initiating the growth of the internal boundary layer seems to be an abrupt change in surface curvature. Once formed, the internal boundary layer dictates the skin-friction distribution and the process of separation over the hill. The effect of the perturbation in wall curvature appears to be different from that due to prolonged convex curvature in that the former affects the flow in the vicinity of the wall instantly, while the latter affects the flow far away from the wall only after the flow turns through some angle. Physical explanations are offered for the qualitative difference between the effects of mild and strong convex curvature, and for the saturated behaviour observed in strongly curved flows. Finally, the results are compared with the behaviour of wind flow over terrestrial hills. In both cases, the internal layer dominates the flow behaviour, even though the scaling laws for the flows over actual hills are not obeyed in the present case. A qualitative comparison reveals that the present internal layer is thicker than that reported in meteorological flows. This appears to be due to the effect of curvature, which perturbs the wake region of the internal layer in the present hill flow, while in meteorological studies the effect of curvature is generally small enough to be neglected.

1. Introduction

The 1980–81 Stanford Conference (Kline, Cantwell & Lilley 1982) demonstrated that many shear flows could not be predicted adequately by existing calculation methods. Most of these flows were distorted or interacting shear layers, otherwise known as

† Present address: Dept. of Aeronautics, Imperial College, London SW7 2BY, UK.
‡ Present address: Dept. of Mechanical & Aerospace Eng., Princeton University, NJ 08544, USA.

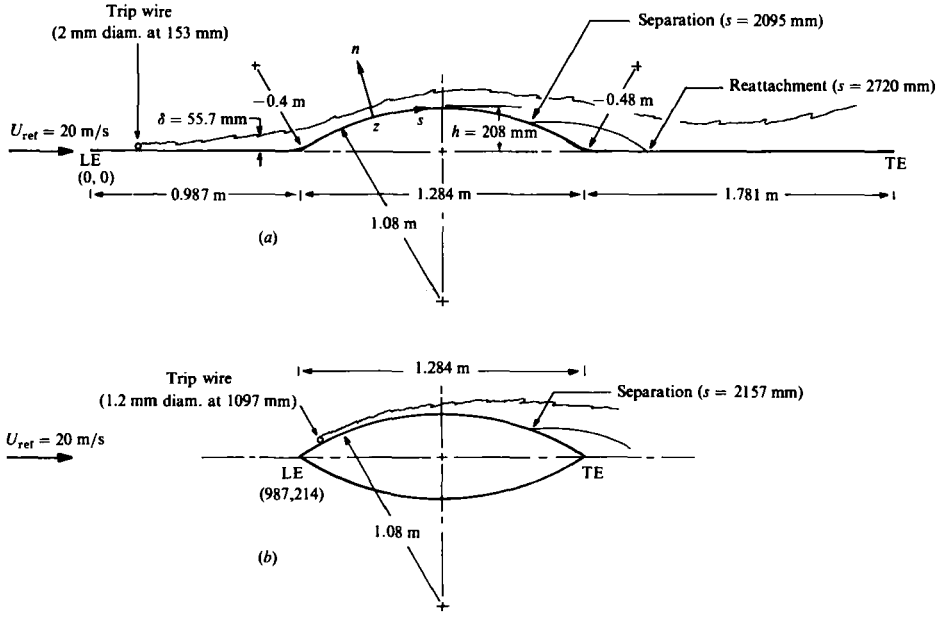

FIGURE 1. Experimental flow configurations. (*a*) Two-dimensional curved hill; (*b*) free wing. LE, leading edge; TE, trailing edge.

'complex' flows. In recent years, therefore, considerable attention has been focused on complex flows, and their behaviour under different extra strain rates (rates of strain additional to simple shearing) has been the subject of many experimental investigations (see, for example, Dumas & Fulachier 1982). These extra strain rates include those due to severe pressure gradients, streamline curvature and divergence, system rotation, bulk compression, separation and reattachment.

Here, we present experimental results obtained in two complex flows involving pressure gradients, streamline curvature and separation. In the first experiment, a turbulent boundary layer flows over a two-dimensional curved 'hill' (see figure 1*a*). The boundary layer forms on a flat plate and then experiences a short region of concave curvature before encountering a prolonged region of convex curvature. The corresponding pressure gradient changes from adverse to favourable and back to adverse, and eventually the flow separates. In the second experiment, a turbulent boundary layer forms on a 'free wing' (figure 1*b*). Here, the boundary layer experiences only convex curvature, and the pressure gradient changes from favourable to adverse. Again, the flow eventually separates. The wing has the same profile as the hill, and over the convex region the streamwise pressure distributions for the two cases, shown in figure 2, display only small differences. (The small jump at the summit appears to be real, since it disappeared during an attempt to set a zero pressure gradient over the hill using flexible sidewalls.) The difference between the two configurations is the finite boundary-layer thickness at the foot of the hill. As a result, at the point of maximum height, the ratio of shear-layer thickness to radius of curvature δ/R is approximately 0.05 on the curved hill and 0.012 on the free wing.

The work reviewed by Bradshaw (1973) demonstrated that a small amount of streamline curvature can have a significant effect on the behaviour of a turbulent flow, and that the effect could be characterized by the 'curvature parameter' δ/R. Small amounts of convex curvature ($\delta/R \approx 0.01$), for example, significantly reduce

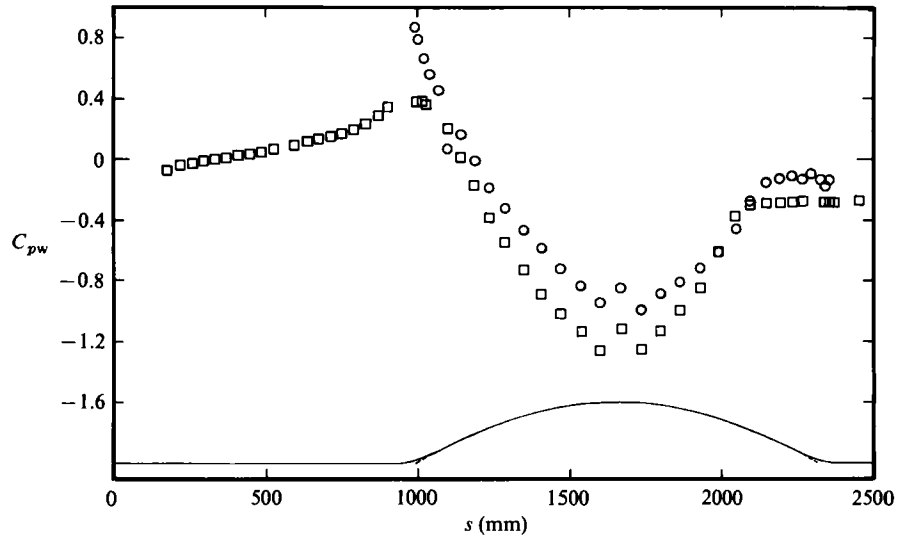

FIGURE 2. Wall-static-pressure distributions: □, curved hill; ○, free wing.

the skin-friction and heat-transfer coefficients (5–15 %). However, recent experiments on strong convex curvature have shown that for $\delta/R > 0.04$ the flow response appears to reach a 'saturated' state (see Gillis & Johnston 1983 or Baskaran 1983 for a review).

In the two experiments considered here, the curvature effects range from mild to strong, and the results show that an 'internal layer' forms in the flow over the hill. This layer shares many similarities with the boundary layer on the free wing, despite the differences in the initial boundary-layer development and the external flow conditions. It appears that the internal layer dictates the overall flow behaviour on the hill almost independently of the external-flow presence. Similar internal layers appear to be responsible for the saturated behaviour observed in strongly curved flows. In this paper, Part 1, we examine the similarities between the two flows and discuss the implications for a wider understanding of the effect of convex curvature. The behaviour of the hill flow was discussed in detail by Baskaran (1983), and the effect of streamline curvature as such will be presented separately as Part 2.

Internal layers have been widely observed in turbulent boundary layers suffering perturbations (Tani 1968; Smits & Wood 1985) and they are associated with abrupt changes in local wall boundary conditions such as roughness, suction or blowing, wall heat flux, surface curvature or by a change in streamwise pressure gradient.

A change in streamwise pressure gradient initially affects the flow in the inner or wall region of the boundary layer, while leaving the flow in the outer or wake region largely unaffected. The response of the inner region depends on the strength and the sense of the pressure gradient, which in turn determines the state of the flow (turbulent or non-turbulent, attached or separated). Under moderate conditions (that is, when the logarithmic law of the wall continues to hold after the perturbation), a sudden change of streamwise static pressure changes the velocity gradient and the turbulent stresses in the inner region, and this modified flow forms an internal layer. Under strong conditions, the behaviour differs considerably from that described above, and separation or relaminarization can occur.

Internal layers in strongly accelerated flows were discussed by Blackwelder &

Kovasznay (1972), and Narasimha & Sreenivasan (1973). In these flows, the stabilizing influence of a favourable pressure gradient causes the flow in the inner region to adopt a quasi-laminar state, via a reverse transitional state. Consequently, the logarithmic region vanishes. When the favourable pressure gradient is completely relaxed, the flow reverts to the turbulent state as indicated by the reappearance of the logarithmic region, accompanied by a large increase in the intermittency and Reynolds stresses close to the wall, and a new internal layer was shown to grow following a natural laminar–turbulent retransition.

Because the nature of the internal layer is different under moderate and strong conditions, we label them as internal layers of the first and second kind, respectively. The total head and the turbulent stresses change rapidly along a mean streamline inside the internal layer in both kinds, while these quantities remain nearly frozen along an outer-layer streamline. Structural parameters, such as the ratio of the shear stress to the turbulent kinetic energy, appear to be almost unaffected over most of the shear-layer thickness.

When the sign of the pressure gradient changes more than once, as in the work of Tsuji & Morikawa (1976), new and different phenomena appear. In that work, a turbulent boundary layer on a flat plate experienced a streamwise pressure gradient alternating in sign (zero to adverse, to favourable, to adverse, to favourable). To begin with, the flow in the inner region was perturbed by the adverse pressure gradient, and in the subsequent favourable-pressure-gradient region the logarithmic law of the wall disappeared. When the pressure gradient changed sign again to adverse, an internal layer appeared and 'knee points' formed in the profiles of Reynolds stresses. The recovery of the law of the wall was slow and occurred when the pressure gradient again changed sign from adverse to favourable farther downstream (about 25 initial-boundary-layer thicknesses).

In contrast to the widely observed existence of internal layers in flows perturbed by changes in pressure gradient, the existence of internal layers in curved flows is not yet a well established phenomenon. The notion of a 'sub-boundary layer' was suggested by Bradshaw (1973) in connection with the strongly curved flow of So & Mellor (1972). More recently Gillis & Johnston (1983) described the growth of an 'active shear-stress layer' following the application of strong convex curvature in a zero pressure gradient. This layer was shown to dominate the whole flow behaviour, and it was suggested that it formed as a result of the reduction in lengthscale in the outer region. However, the changes in the outer layer were not observed till the flow had turned through 13° (Gillis & Johnston 1983, figure 9), while changes in the inner region appeared at the onset of curvature. The changes in the outer layer followed later, even though the effects of streamline curvature were stronger there.

The internal layer in the present hill flow is different from all the internal layers described so far, in that it begins to grow in a region of a strong favourable pressure gradient and surface curvature change (concave to convex), where the normal stresses change across the whole layer rather than simply in the inner region. In addition, the flow in this region is in a reverse transitional state and the law of the wall is absent. We present evidence to show that the internal layer grows as an independent developing boundary layer surrounded by an external free turbulent flow, suggesting a bifurcation of the initial boundary-layer structure. The primary perturbation responsible for triggering the internal layer appears to be the abrupt change in surface curvature.

The configuration shown in figure 1(*a*) resembles the flow over a hill, and comparisons with meteorological studies are of some interest. These studies include

experimental work (Britter, Hunt & Richards 1981; Bradley 1980) and theoretical studies (Jackson & Hunt 1975; Taylor 1977). The flow behaviour was shown to be dominated by the perturbations that occur in an internal layer, whose thickness is given by the height above the hill surface where the perturbation in the mean velocity is a maximum. Since the present hill experiment was designed to investigate the effect of curvature, the scaling laws for the flow over hills were not obeyed. For instance, the ratio of the upwind boundary-layer thickness to the height of the hill $\delta/h \gg 1$ in the above-cited studies, while it is only 0.4 in the present case. However, in all the hill flows it is the internal layer that dominates the flow behaviour, and therefore a qualitative comparison with the present results is given in §5.

2. Apparatus and techniques

The work was carried out in the large, closed-return wind tunnel at Melbourne University. The working section is octagonal, measuring 1.68 m × 1.3 m with a length of 6.54 m. The walls are slotted along the entire length of the working section with an open-to-closed area ratio of 4.9 % to reduce wall interference effects. The adjustable sidewalls were set to give a negligible longitudinal pressure gradient along the centreline of the empty tunnel. The free-wing model was a 32 % thick biconvex airfoil with a radius of curvature of 1.08 m and a chord length of 1.284 m. The curved-hill model was constructed by attaching two flat plates 0.987 m and 1.781 m long to the leading and trailing edges of the free wing. The corners between these plates and the free wing were faired to give radii of curvature of −0.4 and −0.48 m respectively (see figure 1*a*). The models were positioned vertically and the slots in the roof and floor of the tunnel were sealed to prevent end leakage.

Trip wires were used to promote transition. A 1.2 mm diameter trip wire was located 110 mm from the leading edge of the free wing, and for the curved hill a 2 mm diameter trip wire was located 153 mm from the leading edge of the front flat plate. The measurements were taken at a nominal free-stream velocity of 20 m s^{-1} ($U_{\mathrm{ref}}/\nu = 1.33 \times 10^6$ m^{-1}). Skin-friction coefficients were obtained using Preston tubes with the calibration of Patel (1965), and Clauser charts using constants of 0.41 and 5.2 (de Brederode & Bradshaw 1974). The mean flow field was explored using Pitot tubes, and the wall distance was corrected for displacement effects by the addition of 15 % of probe diameter. Turbulence measurements were made using Melbourne University unlinearized constant-temperature hot-wire anemometers. Both normal and crossed hot wires were employed. All measurement locations were referred to a (s, n, z) curvilinear coordinate system fixed in the surface of the model with its origin at the leading edge of the front flat plate. The measurement locations on the free wing were also referred to this origin (see figure 1).

Some measurement procedures in the two experiments were slightly different. For the flow over the free wing, the Preston tube diameters were 0.6 mm and 1.07 mm. Mean velocity profiles were obtained using a flattened Pitot tube with a height of 0.34 mm. The local mean static pressure p varied with wall distance n because of streamline curvature, and it was calculated from the wall static pressure p_{w} using Bernoulli's equation in the normal direction and the irrotationality condition. So & Mellor (1972) showed that with these assumptions $U_{\mathrm{p}} = U_{\mathrm{pw}} \mathrm{e}^{kn}$ for $k \ll n$, where U_{p} is the local potential velocity, U_{pw} is the potential velocity at the wall and k is the curvature of the surface (positive for convex and negative for concave curvature). To measure the turbulence levels, a DISA 55P05 normal-wire probe was used. The wire was statically calibrated before and after every profile using the

power-series approach given by Perry (1982), and temperature corrections were applied using the method of Abell (1977). No crossed-hot-wire measurements could be conducted with free-wing experiment because the boundary layer was too thin for adequate spatial resolution.

In the case of the curved hill, the Preston tube diameters were 1.08 mm and 1.26 mm, and a round Pitot tube of 0.5 mm diameter was used. The static pressure across the boundary layer was measured using a 1 mm thick disc-static probe of 10 mm diameter since the method of So & Mellor (1972) was found to be invalid in the regions where the surface curvature changes abruptly. The normal and crossed-wire probes were manufactured in-house. In each case, Wollaston wires were soldered to the probe and etched to give a filament diameter of 5 μm with an active length of 1.2–1.5 mm. The crossed-wire probe could be rotated accurately about its axis through 90°, enabling measurements in two perpendicular planes (referred to as the '*UV* Mode' and '*UW* Mode') to be made at a point. A dynamic calibration procedure (Perry 1982) was adopted for both normal and crossed wires. For normal wires, the dynamic calibration procedure uses the same power-series approach employed during the static calibration in the free-wing experiment, and the maximum difference in $\overline{u^2}$ using these two methods is approximately 4 % (Perry 1982). The crossed-hot-wire probe was pitch aligned so that the ratio of the normal component of velocity to the streamwise component in the measurements near the wall matched that observed in the calibration. All calibrations and measurements were carried out on-line using a PDP11/10 digital computer equipped with an analog-to-digital converter. For each wire, four sets of 8000 samples were collected at a sampling frequency of 200 Hz. Further details of the calibration and data reduction procedures as well as tabulations of data for the hill flow are given in Baskaran & Joubert (1984). During the calibration, it was found necessary to filter the hot-wire signals at a frequency that is at least one decade above the shaking frequency of the calibrator, to avoid noise pick-ups due to vibrations. In order not to change the gain of the circuit during measurement the filter was retained and the low-pass frequency was altered to the maximum available, namely 10 kHz.

3. Results and discussion

3.1. *Free wing*

The skin-friction coefficients over the free wing are shown in figure 3. The values inferred from the Clauser chart generally agree to within 2 % with those obtained using the 0.6 mm Preston tube, except near the trip wire and the separation point (for $s > 2000$ mm the error in C_f is approximately 15 %). The separation point was found to lie at $s = 2157$ mm by extrapolating the skin friction values to zero. The calculation method of Bradshaw & Unsworth (1974), which includes an empirical factor for the effects of curvature, fails to predict separation. In addition, the skin-friction values are overestimated somewhat.

The other integral parameters are shown in figure 4. The displacement and momentum thicknesses are defined as

$$\delta^* = \int_0^\infty \left(1-\frac{U}{U_p}\right) \mathrm{d}n; \quad \theta = \int_0^\infty \frac{U}{U_p}\left(1-\frac{U}{U_p}\right) \mathrm{d}n.$$

The wavy nature in the initial variation of the boundary-layer thickness δ (the wall distance at which the dynamic pressure is 99 % of the free-stream value) is probably

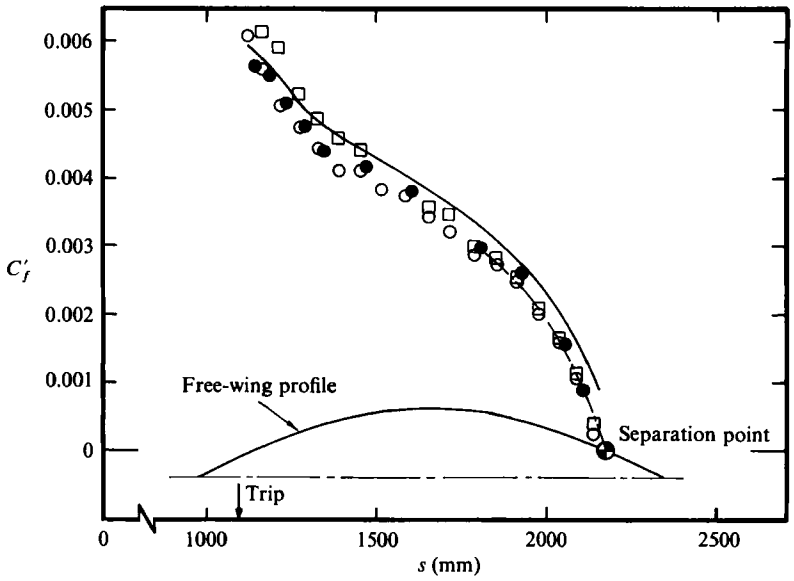

FIGURE 3. Skin-friction distribution over free wing. Preston tube: ○, 0.6 mm; □, 1.067 mm; ●, Clauser chart; ——, calculation (Bradshaw & Unsworth 1974); ——— line for extrapolation.

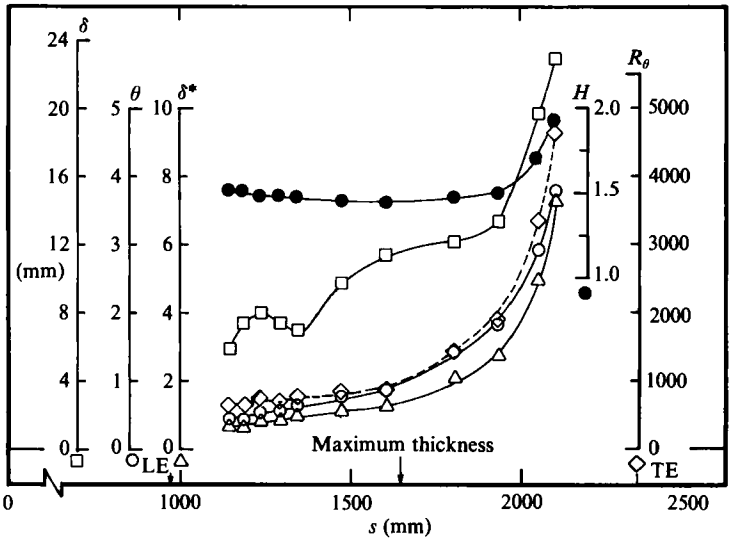

FIGURE 4. Integral parameters for free wing: □, boundary-layer thickness; ○, momentum thickness; △, displacement thickness; ●, shape parameter; ◇, momentum-thickness Reynolds number.

due to the influence of the trip wire. The same variation appears in the displacement and momentum thicknesses, but with a much smaller amplitude. All these parameters grow rapidly as the flow approaches separation. The shape parameter H however remains at a constant value of 1.5 over most of the flow, indicating that the profiles are not greatly distorted except close to separation (1.5 is a typical value at this Reynolds number). R_θ is less than 5000 everywhere and low-Reynolds-number effects may be important (Coles 1962).

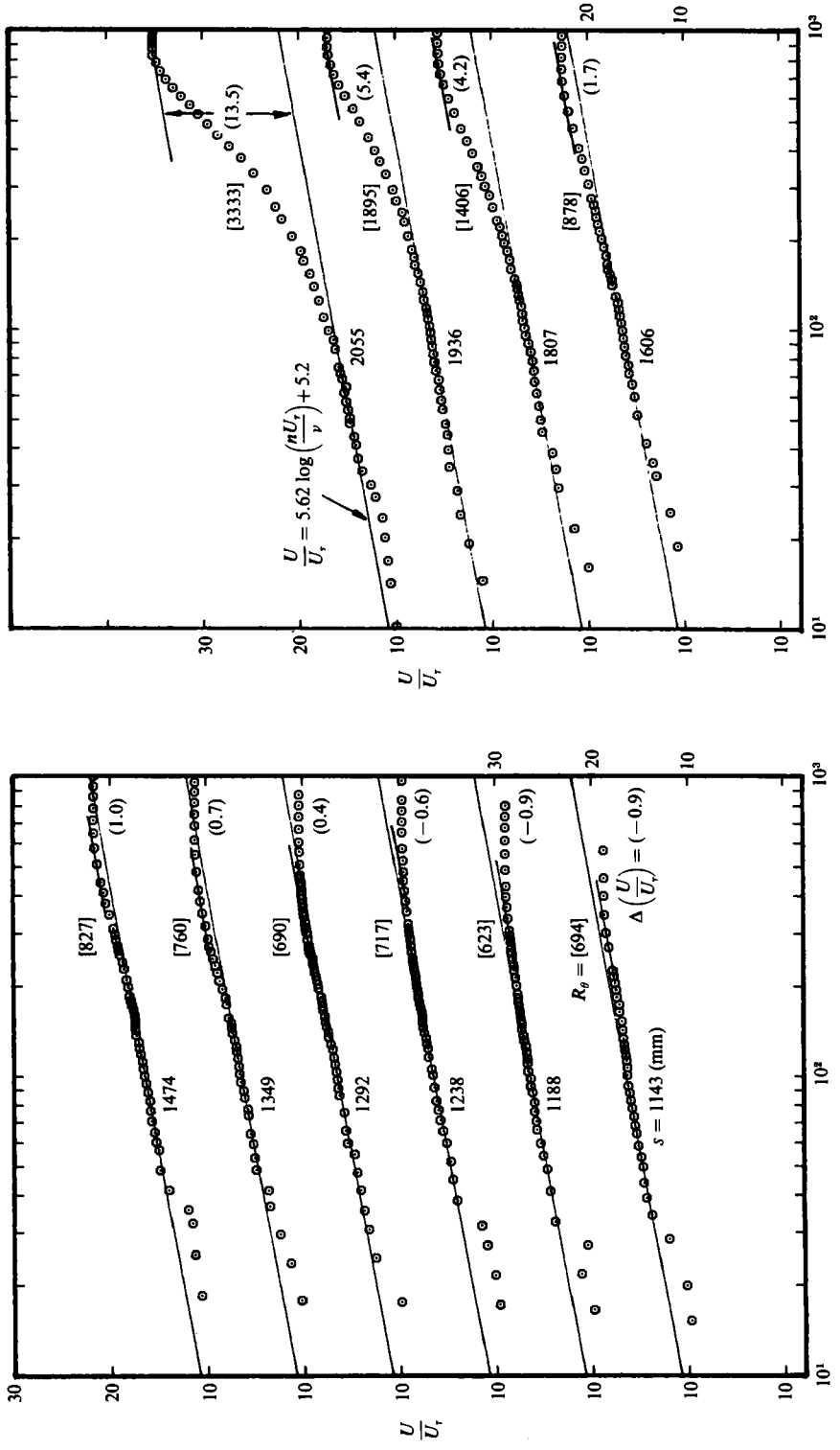

FIGURE 5. Mean velocity profiles for free wing. Note the shift in the ordinate scale.

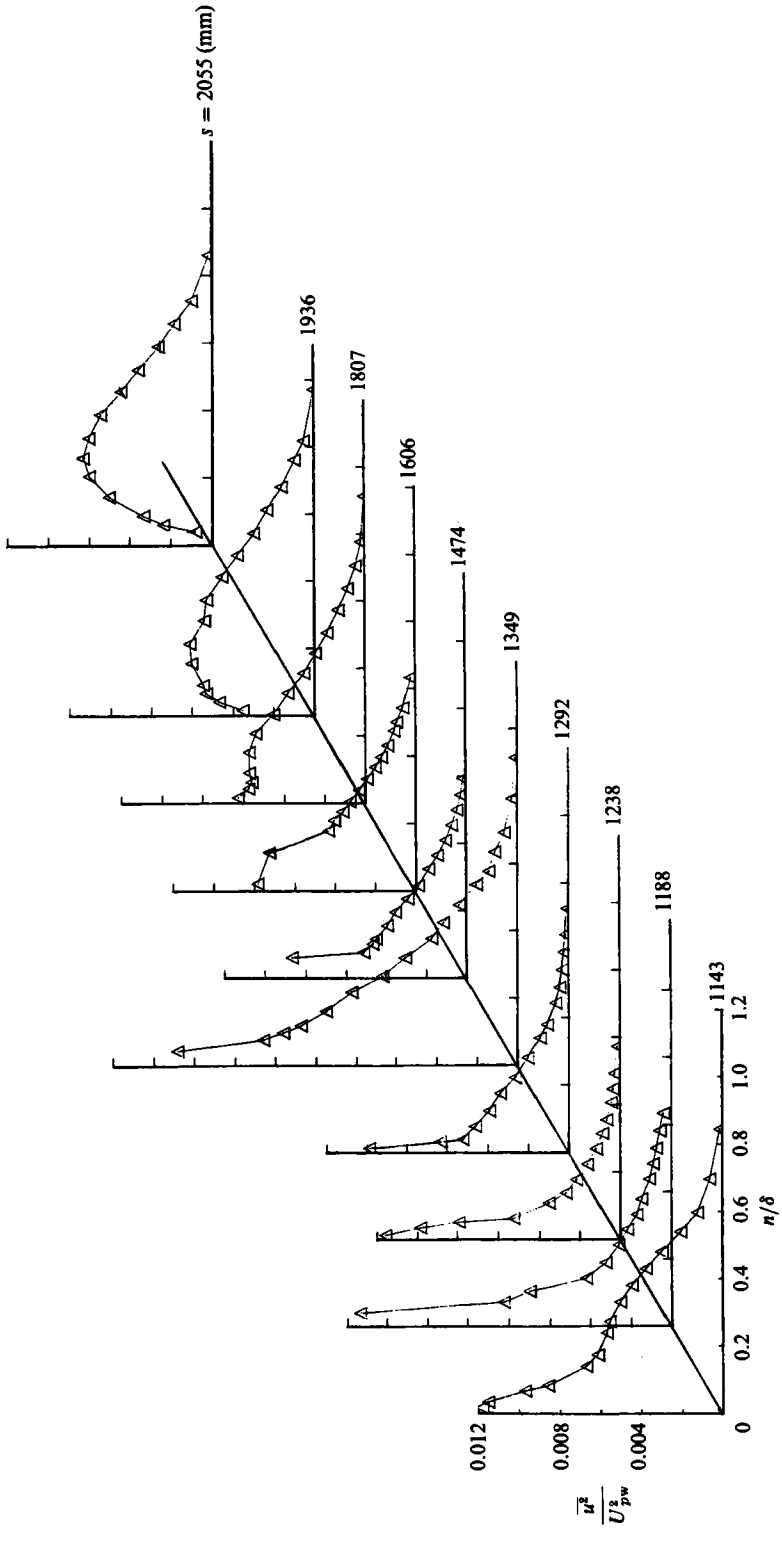

FIGURE 6. Profiles of $\overline{u^2}/U_{pw}^2$ for free wing.

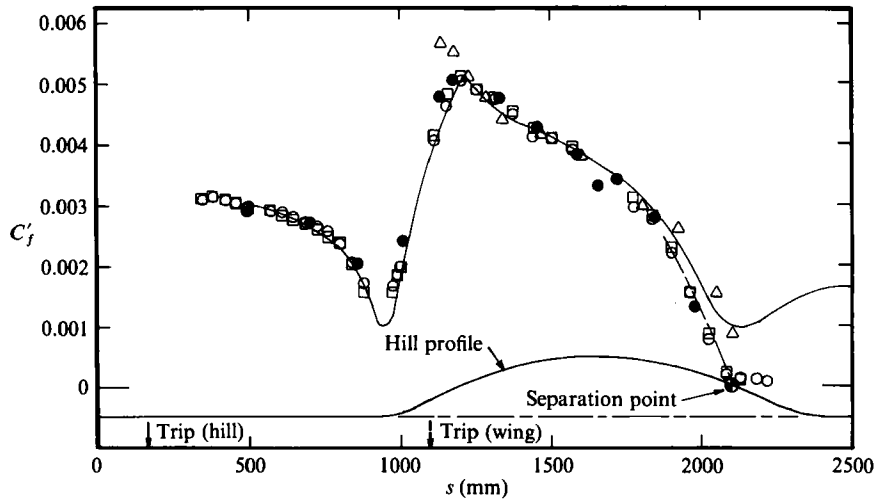

FIGURE 7. Skin-friction distribution over curved hill. Preston tube: ○, 1.083 mm; □, 1.261 mm; ●, Clauser chart; ——, calculation (Bradshaw & Unsworth 1974); ———, line for extrapolation; △, free wing.

The mean velocity profiles in wall coordinates are shown in figure 5. The logarithmic region is reasonably extensive at all locations, despite the effects of severe pressure gradients, convex curvature and low Reynolds number. In contrast, the wake component is affected greatly. In the region of favourable pressure gradient, the wake factor, $\Delta(U/U_\tau)$, varies from -0.6 to 1.0, and it is generally smaller than the constant-pressure-layer values (0.9–1.2) reported by Coles (1962), Purtell, Klebanoff & Buckley (1981) & Smits, Matheson & Joubert (1983) in the same Reynolds-number range (623–878). The behaviour of the wake factor is due mainly to the severe favourable pressure gradient since convex curvature would tend to increase the wake factor. In any case, δ/R is too small in this region (0.005) to have any significant effect on the wake factor.

In the region of adverse pressure gradient, the wake factor increases to values much greater than the constant-pressure-layer values of approximately 2.0 at the same R_θ. Both adverse gradient and convex curvature tend to increase the wake factor. However, Muck, Hoffmann & Bradshaw (1985) found that after an application of prolonged convex curvature ($\delta/R = 0.01$), the wake factor increased only from 1.0 to 2.2. Therefore, the behaviour of the wake factor everywhere on the free wing reflects the dominant influence of pressure gradient.

The profiles of longitudinal turbulent intensity $\overline{u^2}$ scaled with respect to $U_{\rm pw}[=U_{\rm ref}(1-C_{pw})^{\frac{1}{2}}]$ are shown in figure 6. Since the effects of curvature are small, the results reflect the influence of pressure gradient. As expected, therefore, the intensities are reduced in the region of favourable pressure gradient ($s > 1630$ mm).The overshoot in the intensity at $s = 1349$ mm is repeatable and it is probably related to the wavy behaviour of the integral parameters close to the trip wire. Such behaviour is often observed during the later stages of transition (Castro & Bradshaw 1976). The profiles in the region $s > 1630$ mm are typical of those observed in turbulent boundary layers experiencing adverse pressure gradients. The main feature is the presence of a maximum which propagates towards the edge of the boundary layer as the strength of the pressure gradient increases.

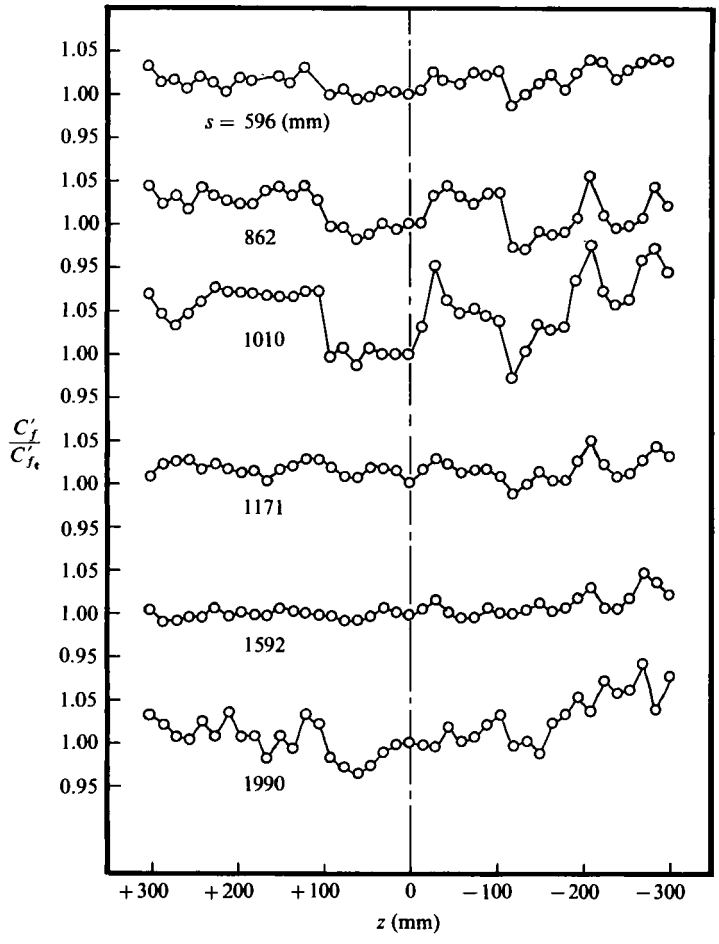

FIGURE 8. Spanwise variation of skin friction for curved hill.

3.2. *Curved hill*

The skin-friction coefficients are shown in figure 7. The values inferred from the Clauser chart are again found to agree with the Preston-tube values to within 2% everywhere, except in the region where the surface curvature changes from concave to convex (called the 'exit' region) and close to separation (for $s > 1862$ mm, C_f is accurate to about 13%). The location of the separation point is found to lie at $s = 2095$ m by extrapolation. The skin friction over the leading-edge plate decreases due to the increasingly adverse pressure gradient, as expected. The values over the concave portion generally follow the trend of the pressure gradients. Further downstream, the behaviour is similar to that observed on the free wing. The agreement between the method of Bradshaw & Unsworth (1974) and the experiment is reasonable, considering the complexity of the flow. However, the method again fails to predict separation.

The spanwise variation of skin friction is shown in figure 8. The variation of about 2% at $s = 596$ mm is possibly due to the tunnel screens. These inhomogeneities are amplified at the foot of the hill and the maximum amplification occurs in the concave

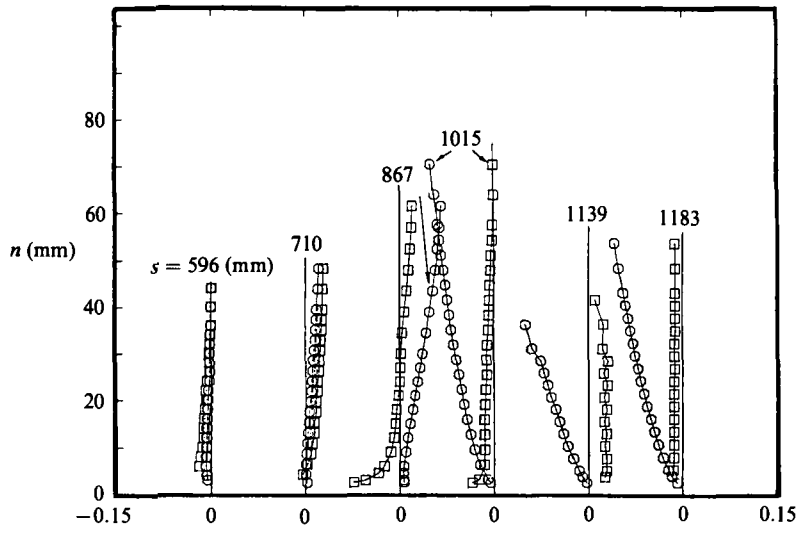

FIGURE 9. Profiles of V and W around the concave bend over curved hill (leading-edge plate: $s = 596$ mm; 710; 867; concave bend: 1015; exit: 1139; 1183). ⊖, V/U_{pw}; ⊟ W/U_{pw}. Note shift in abscissa scale.

section (this is not due to the decrease in the scaling value). A rapid attenuation follows over the region of convex curvature.

It appears that secondary flows exist in the region of concave curvature. However, the spanwise variation of C_f does not exhibit any regular spatial periodicity consistent with the presence of Taylor–Görtler vortices, as commonly observed in boundary layers over concave surfaces (Smits, Young & Bradshaw 1979*b* and Hoffmann, Muck & Bradshaw 1985). The absence of Taylor–Görtler vortices is also indicated by the measurements of Reynolds shear stresses, $-\overline{uv}$ and $\overline{uw}$ (Baskaran & Joubert 1984), which do not vary in the spanwise direction. Instead, the secondary flow appears to be due to yawing of the mean streamlines, as indicated by the profiles of W shown in figure 9. This cross-flow appears to prevent the formation of Taylor–Görtler vortices. Hall (1984) showed that a similar suppression of Taylor–Görtler vortices in a three-dimensional laminar boundary layer over a concave surface was due to the dominance of the 'cross-flow' instability mode over the Taylor–Görtler instability mode. One of us (V.B.), currently investigating a three-dimensional turbulent boundary layer over a concave surface at Imperial College, has also observed the absence of Taylor–Görtler vortices. In the present case, since the vortices are not formed over the concave region initially, whether a convex curvature following a concave surface can suppress these vortical motions is still open to question. In any case, the inhomogeneities amplified in the bend are attenuated over the convex region, giving the mean flow a tendency towards two-dimensionality.

The integral parameters, shown in figure 10, all show dramatic changes in the concave region. In the convex region, the shape parameter falls to a value as low as 1.1, indicating that the profiles are considerably distorted. The static-pressure profiles (figure 11) show that the normal pressure gradients follow the sense of the surface curvature (positive for convex and negative for concave). The profiles of V, shown earlier in figure 9 change sign between the foot of the hill and the concave bend.

The mean velocity profiles (figure 12) display a well-defined logarithmic region, except in the concave bend and in the exit region. The dip below the logarithmic law

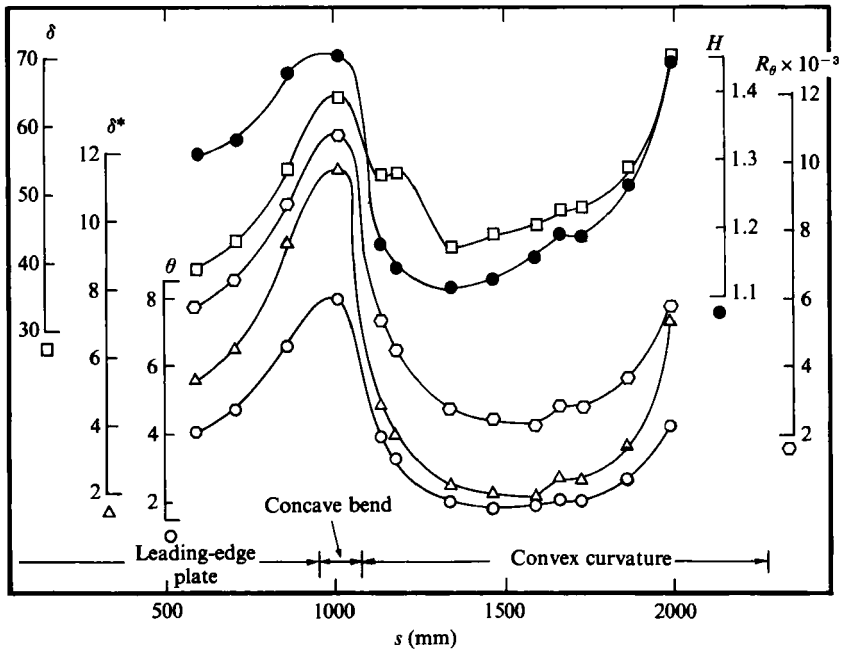

FIGURE 10. Integral parameters for curved hill: □, boundary-layer thickness; ○, momentum thickness; △, displacement thickness; ●, shape parameter; ⬡, momentum-thickness Reynolds number.

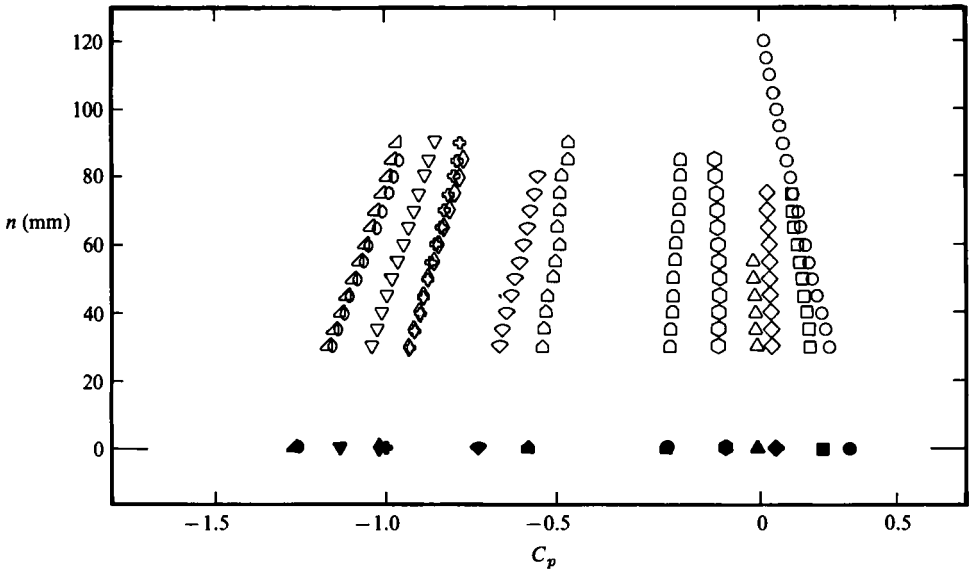

FIGURE 11. Static-pressure profiles for curved hill (solid symbols refer to wall). Leading-edge plate: △, $s = 596$ mm; ◇, 710; □, 867; concave bend: ○, 1015; exit: ⬡, 1139; ⬭, 1183; convex curvature: ◇, 1345; ◇, 1469; ⬯, 1596; ▽, 1665; ⊿, 1730; ◈, 1862; ⌂, 1990.

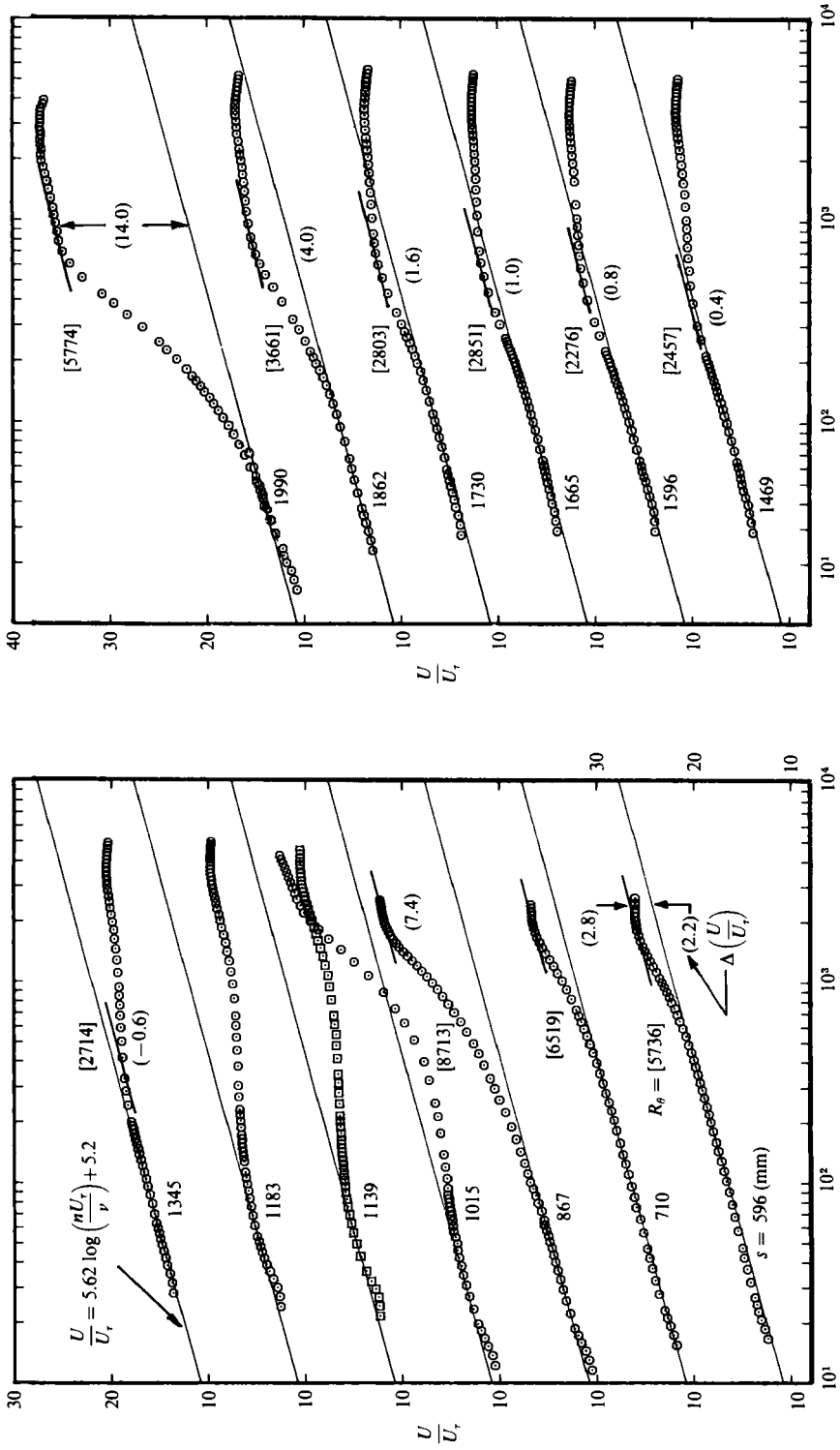

FIGURE 12. Mean velocity profiles for curved hill. Note shift in ordinate scale.

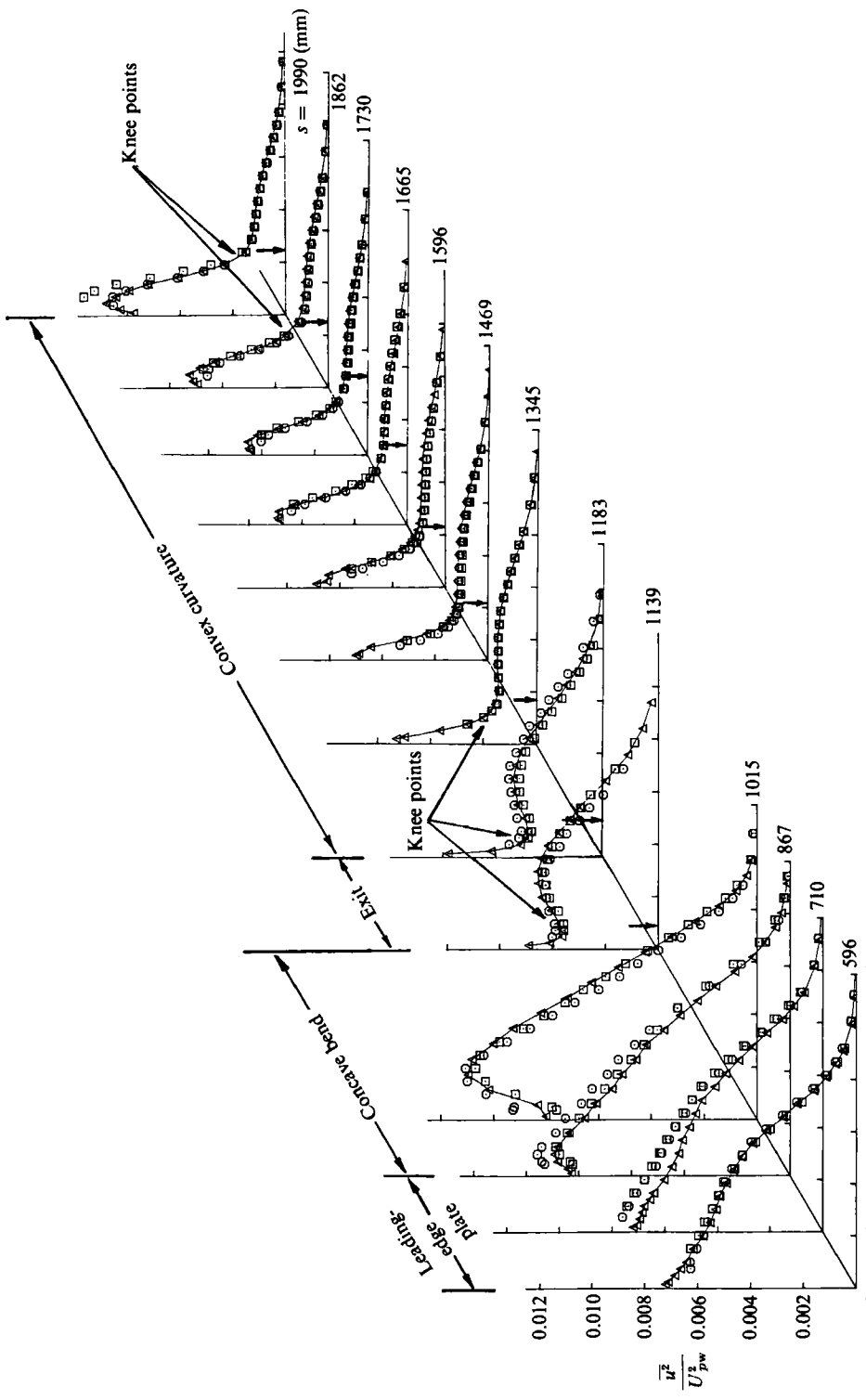

FIGURE 13. Profiles of $\overline{u^2}/U_{pw}^2$ for curved hill (arrows on abscissa indicate the location of free-wing boundary-layer edge): △, normal wire. Crossed wires: ○, *UV* Mode; □, *UW* Mode.

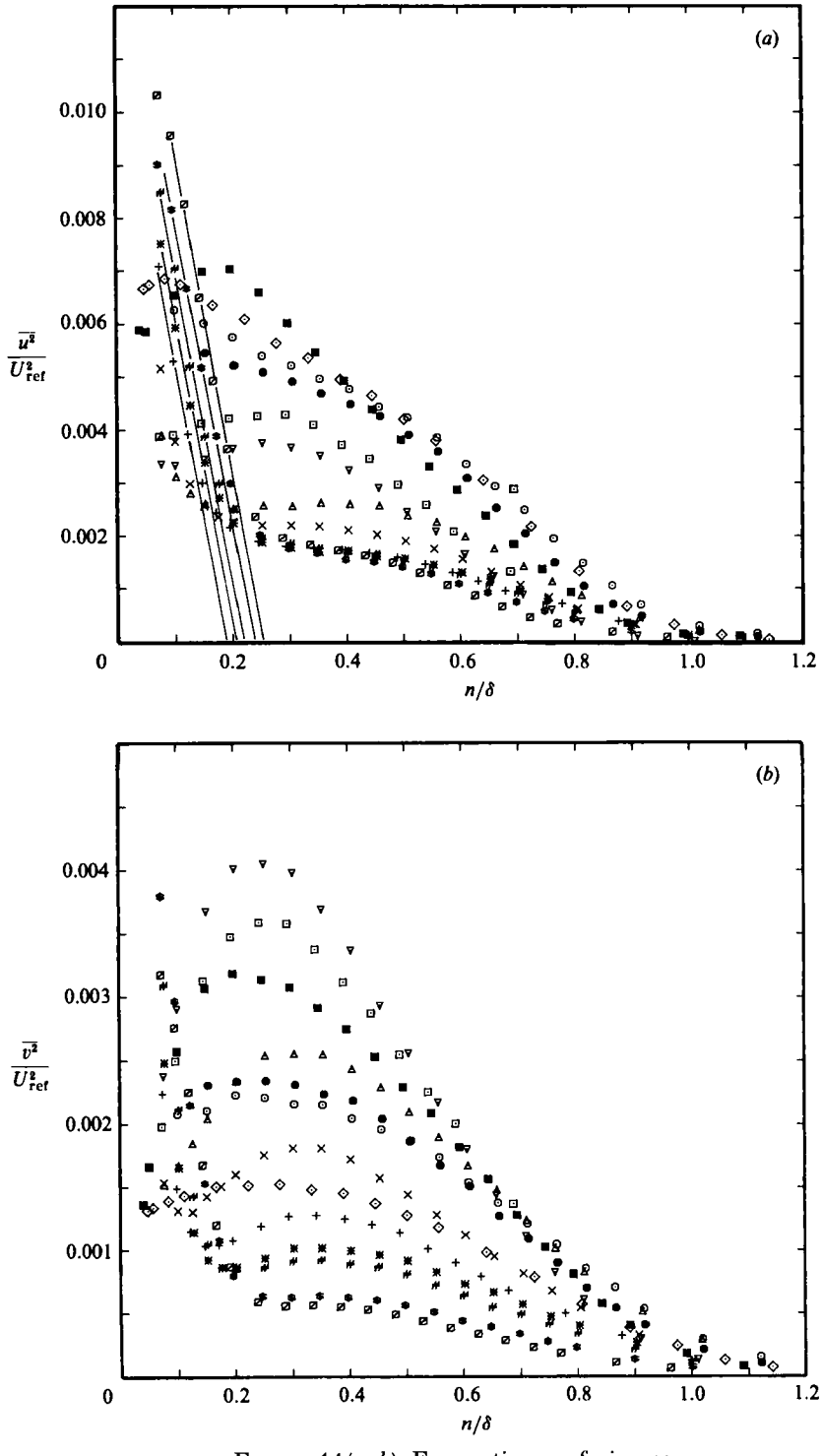

FIGURE 14(*a*, *b*). For caption see facing page.

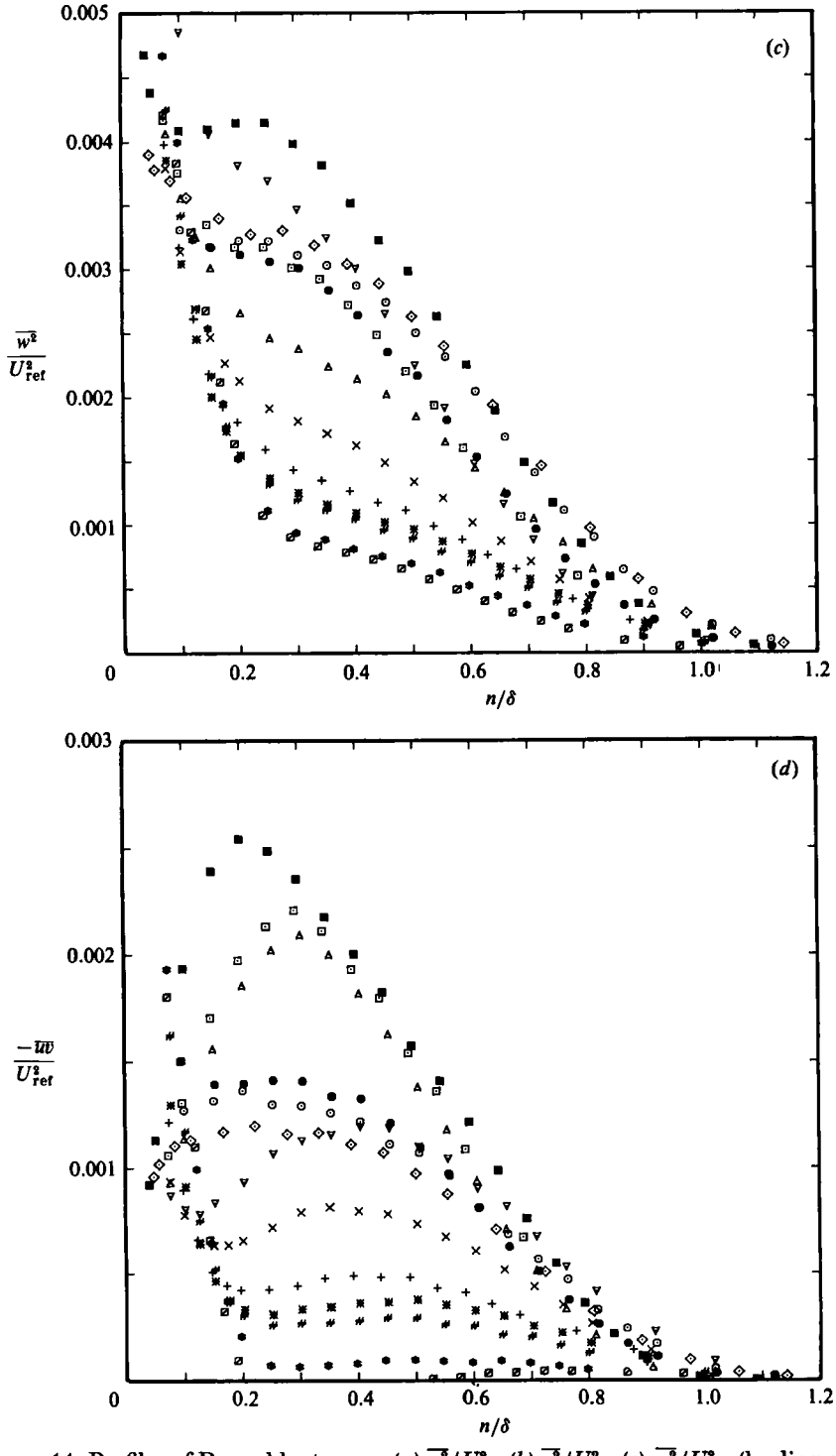

FIGURE 14. Profiles of Reynolds stresses. (*a*) $\overline{u^2}/U_{\rm ref}^2$ (*b*) $\overline{v^2}/U_{\rm ref}^2$ (*c*) $\overline{w^2}/U_{\rm ref}^2$ (leading-edge plate: ●, $s = 596$ mm; ○, 710; ◇, 897 (foot of the hill); concave bend: ■, 1015; exit: □, 1139; ▽, 1183; convex curvature: △, 1345; ×, 1469; +, 1596; *, 1665; #, 1730; $, 1862; ∅, 1990). (*d*) $-\overline{uv}/U_{\rm ref}^2$: △, 1183; ▽, 1345 (symbols for $-uv$ at other stations same as other components). ——, extrapolation to determine δ_1.

in the concave bend has been observed in a wide variety of complex flows (Smits, Eaton & Bradshaw 1979*a*; Smits *et al.* 1979*b*; Hoffmann *et al.* 1985 in concave flows, Chandrsuda & Bradshaw 1981 in a reattaching mixing layer, and Marumo, Suzuki & Sato 1978 in a turbulent boundary layer perturbed by a circular cylinder). These dips are generally interpreted as indicating an increase in the turbulent lengthscale.

At the exit, the values of C_f inferred from the Clauser chart differ by 15% from the Preston-tube measurements. A Preston tube can give erroneous results if its centre lies outside the logarithmic region or if the logarithmic law is violated. In the latter case, even Clauser's method will fail. The observed discrepancy does not appear to be due to the size of the Preston tube since a much smaller one (0.5 mm diameter) still gave approximately the same result. However, Jones & Launder (1972), from a study of sink-flow boundary layers, showed that a universal logarithmic region is not discernible in the velocity profile if the pressure-gradient parameter $K(=-\nu/\rho U_{pw}^3\,\mathrm{d}p/\mathrm{d}x)$ exceeds a value of $+1.0\times10^{-6}$. In the region of the discrepancy, K varies from $+1.7\times10^{-6}$ to $+2.4\times10^{-6}$, and the law of the wall is probably not applicable. Surprisingly, the logarithmic region re-emerges at the next station ($s = 1345$ mm) in a clean and extensive manner, in contrast to the observations of Tsuji & Morikawa (1976), where the recovery of the law of the wall was reported to be slow. Downstream of this location, the increase in the wake factor is in the expected sense. Interestingly, the magnitudes of the wake factor over the convex surface are similar to those on the free wing, and the point of maximum deviation in $\Delta(U/U_\tau)$ occurs at nearly the same (nU_τ/ν) for both flows.

The profiles of $\overline{u^2}$ scaled with respect to the potential wall velocity are shown in figure 13. To identify the absolute changes, the profiles of the normal stress $\overline{u^2}$, $\overline{v^2}$ and $\overline{w^2}$, and the shear stress $-\overline{uv}$, are shown scaled with respect to the reference velocity in figure 14. The profiles over the leading-edge plate at the first two stations are consistent with the behaviour expected in a mild adverse pressure gradient, and the changes are significant only in the inner region ($n/\delta < 0.2$). The behaviour near the foot of the hill where the streamlines are yawed is in qualitative agreement with that observed in three-dimensional boundary layers: $\overline{v^2}$ and $-\overline{uv}$ decrease, and $\overline{w^2}$ increases (Bradshaw & Pontikos 1985). In the concave bend, all stresses increase significantly right across the layer. All components (except $\overline{w^2}$) display a maximum at $n/\delta = 0.2$, similar to that reported by Smits *et al.* (1977*a*). Downstream, these maxima move away from the wall to $n/\delta = 0.3$ at the exit, where the increase in $\overline{v^2}$ persists, while the other two components decrease across the whole layer. In contrast, $-\overline{uv}$ at the exit decreases only below $n/\delta = 0.3$, while it is unchanged in the outer portion of the flow.

The decreases in $\overline{u^2}$ and $\overline{w^2}$ at the exit cannot be attributed to the effect of stabilizing curvature, because $\overline{v^2}$ and $-\overline{uv}$ should also decrease. The results are also inconsistent with the effects of a change in pressure gradient, since the normal stresses change right across the layer rather than just in the inner region. Instead, a redistribution of energy appears to occur among the normal stress components. This redistribution of energy to $\overline{v^2}$ at the expense of the other normal stress components is something not typical of wall layers, where $\overline{u^2}$ and $\overline{w^2}$ usually increase at the expense of $\overline{v^2}$. Rather, the behaviour strongly resembles that of free-shear layers affected by a wall constraint (Castro & Bradshaw 1976; Chandrsuda & Bradshaw 1982; Wood & Bradshaw 1982, 1984).

At the beginning of the convex region, sharp gradients in all the Reynolds stresses appear close to the wall as soon as the logarithmic region reappears, and 'knee points' form in the profiles where these gradients level off. The knee points gradually

propagate towards the edge of the boundary layer as the flow proceeds downstream. Below the knee points, the stresses increase with downstream distance, while outside the knee points all the stresses decrease under the action of prolonged streamline curvature. But this decrease is only gradual, unlike the sudden decrease reported by So & Mellor (1972), Prabhu & Sundarasiva Rao (1981) and Gillis & Johnston (1983) in strongly curved flows. In those flows, the shear stress in the outer region even changed sign near the beginning of convex curvature, whereas in the present case the sign of $-\overline{uv}$ changes only just before separation.

3.3. *Comparison of wing and hill flows*

The two flows exhibit many intriguing similarities and some equally interesting differences. For instance, the skin-friction coefficients are almost equal in the region 1200 mm $< s <$ 1800 mm, while the wake factors are slightly smaller in the hill flow. This is surprising, because the curvature parameter for the hill flow is about five times larger than that for the free-wing experiment and the expected decrease in the skin friction and increase in the wake factor for the hill flow are not observed. Furthermore, the location of the separation points in the two flows differed by only 5% of the free-wing chord. If the effect of convex curvature, as represented by the curvature parameter δ/R is indeed stronger in the hill flow, separation is expected to occur much earlier, since convex curvature suppresses turbulence mixing.

Now, the wake factors are only slightly different in the two flows, while the skin-friction coefficients are nearly the same. But the momentum-thickness Reynolds numbers are widely different, even though the maximum value of U/U_τ occurs almost all the same nU_τ/ν in the two flows. We denote this value of nU_τ/ν as the Coles thickness δ_c. To a first approximation, the skin friction for a flat-plate boundary layer is uniquely determined by the wake factor and the momentum-thickness Reynolds number. The mean velocity profiles over the convex region below δ_c do not appear to be sufficiently abnormal for this first approximation to be invalid, especially given that the pressure gradients are only slightly different. Then, is it possible to have almost the same wake factors at two widely different values of R_θ for a given C_f and streamwise pressure gradient?

Putting that question aside for the moment, a striking feature of the hill flow is that knee points in the Reynolds-stress profiles appear as soon as the logarithmic region recovers over the convex surface. The locations of the knee points almost coincide with the locations of δ_c, and they also move away from the wall in a manner that closely resembles the growth of the boundary layer on the free wing. These observations suggest that (*a*) an internal layer forms in the flow over the curved hill, and (*b*) the free-wing boundary layer is in some sense similar to this internal layer. In fact, the profiles of Reynolds stresses over the convex region of the hill exhibit a compelling resemblance to those generally observed in perturbed boundary layers (see, for example, Tsuji & Morikawa 1976; Andreopoulos & Wood 1982). Initial comparisons between the two experiments showed that the $\overline{u^2}$ data below the knee points in the hill flow at s = 1730 mm and 1862 mm agreed well with the $\overline{u^2}$ profiles on the free wing at s = 1807 mm and 1936 mm respectively, supporting the concept that the internal layer and the free-wing boundary layer are similar but suggesting that the two layers have their origins at different locations. Such a difference in the origins is expected, since there is no tripping device in the convex region of the hill and the pressure-gradient history in the flows is slightly different.

Far downstream, however, the effects due to differences in origin should become negligible, and if these two flows are truly similar any differences in the behaviour

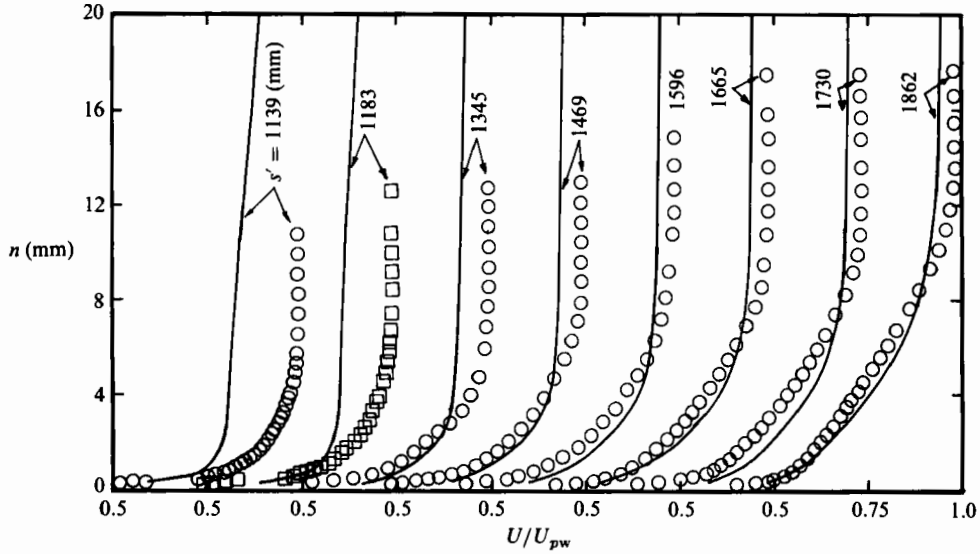

FIGURE 15. Comparison of mean velocity profiles: ——, curved hill; ○, □, free wing (corrected for effective origin). Note shift in abscissa scale.

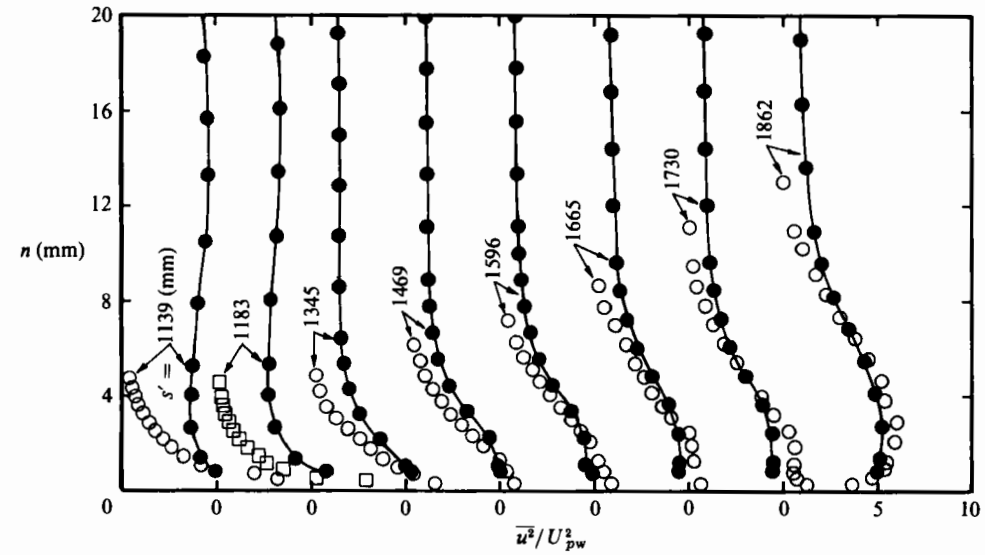

FIGURE 16. Comparison of $\overline{u^2}$ profiles: ●, curved hill; ○, □, free wing (corrected for effective origin). Note shift in abscissa scale.

should reflect the differences in external conditions such as pressure gradients. At the two locations where the initial comparisons were made, the pressure gradient parameters, K or β ($=\delta^*/\rho U_\tau^2\, \mathrm{d}p/\mathrm{d}x$) are nearly equal ($\beta = 2.3$ and 5.3 on the free wing, and 2.8 and 5.8 on the hill respectively; $K = -0.23\times10^{-6}$ and -0.26×10^{-6} on the free wing and -0.2×10^{-6} and -0.3×10^{-6} on the hill, respectively). Therefore, the difference in streamwise location can be used to define a difference in the origin of the two layers, and the hill-flow results are compared with those on the free wing 74 mm further upstream ($s' = s-74$).

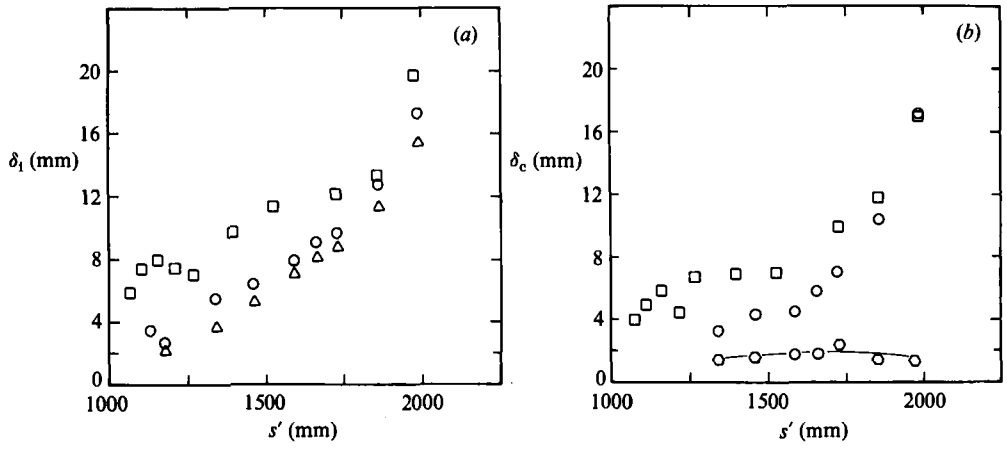

FIGURE 17. (*a*) Internal-layer thickness. δ_i: ○, from knee points; △, from total-pressure–stream function plot; □, free wing (corrected for effective origin). (*b*) Coles' thickness δ_c: ○, curved hill; □, free wing (corrected for effective origin); ⬡, edge of the logarithmic region over the curved hill.

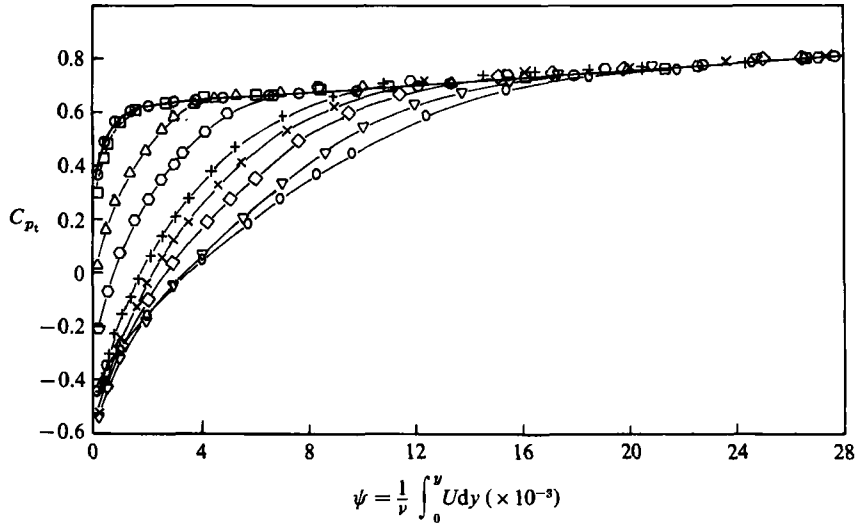

FIGURE 18. Plot of total pressure versus stream function for curved hill. Exit: ○, s = 1139 mm; □, 1183; convex curvature: △, 1345; ⬡, 1469; +, 1596; ×, 1665; ◇, 1730; ▽, 1862; ⬯, 1990.

The mean velocity and turbulent-intensity profiles for the two flows, after correcting for the effective origin, are compared in figures 15 and 16. Where necessary, the free-wing profiles were interpolated to make the comparison at the same streamwise location relative to the effective origin. The results agree more closely as the streamwise distance increases, and the outward spreading of the common region follows the growth of the internal layer in the hill flow. The differences between the initial profiles in the two flows reflect the different upstream histories as well as the differences in the vicinity of the origin. These differences are also apparent in the thicknesses and growth rates of the internal layer and the free-wing boundary layer, shown in figure 17 (*a*). The thickness of the internal layer δ_i is determined from the total-pressure–stream-function plots (figure 18) as well as by linearly extrapolating

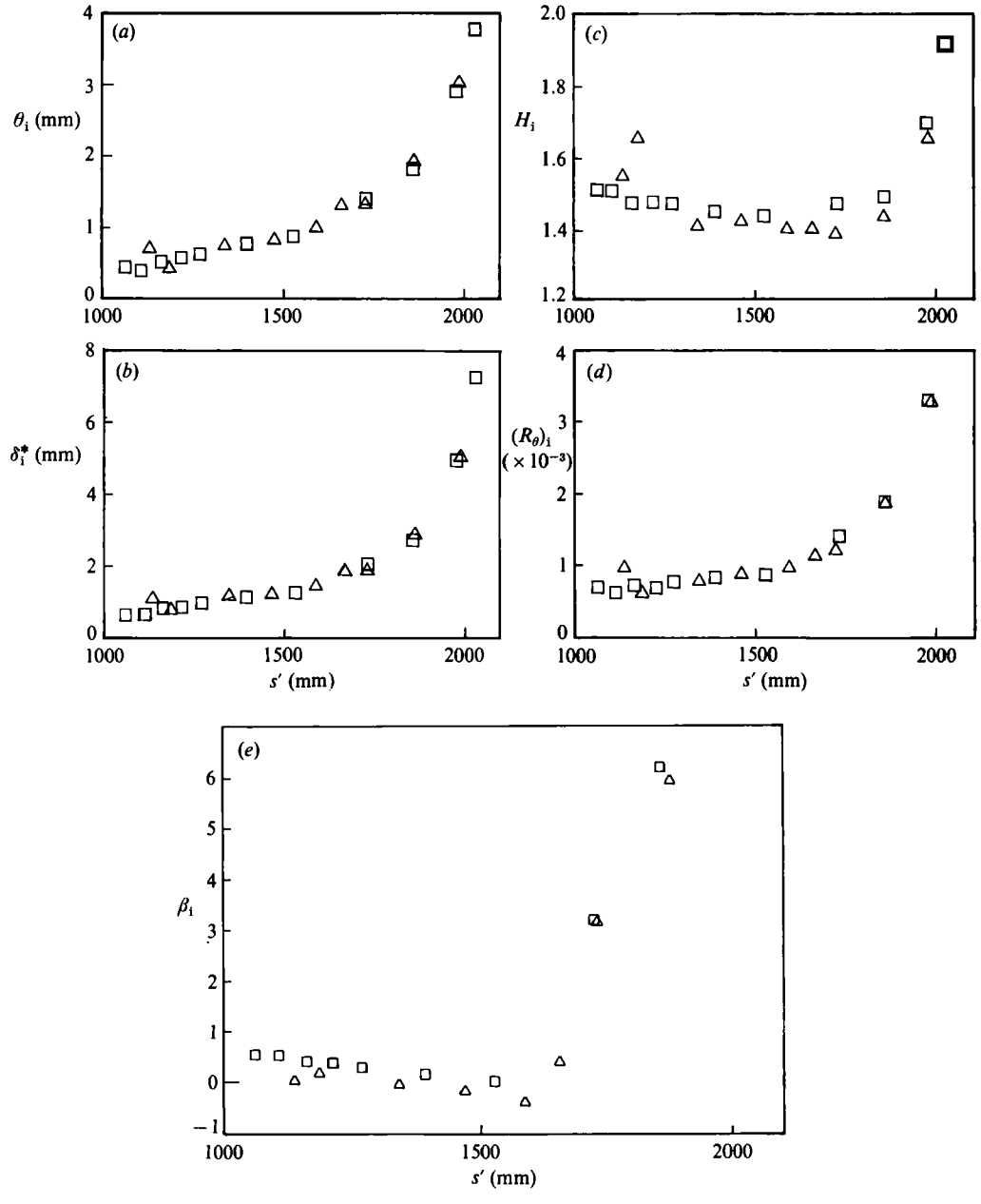

FIGURE 19. Internal-layer integral parameters. (*a*) Momentum thickness; (*b*) displacement thickness; (*c*) shape parameter; (*d*) momentum-thickness Reynolds number; (*e*) pressure-gradient parameter; △, internal layer; □, free wing (corrected for effective origin).

the $\overline{u^2}$ profiles below the knee point to zero (figure 14*a*). The values of δ_i derived from the two methods are slightly different but the overall trend in the growth rates is similar (see figure 17*a*). These trends are not surprising; the internal layer is shrouded by a strong turbulent field, while the free-wing boundary layer is bounded by a potential flow. The streamwise variation of δ_c for the two flows, together with the

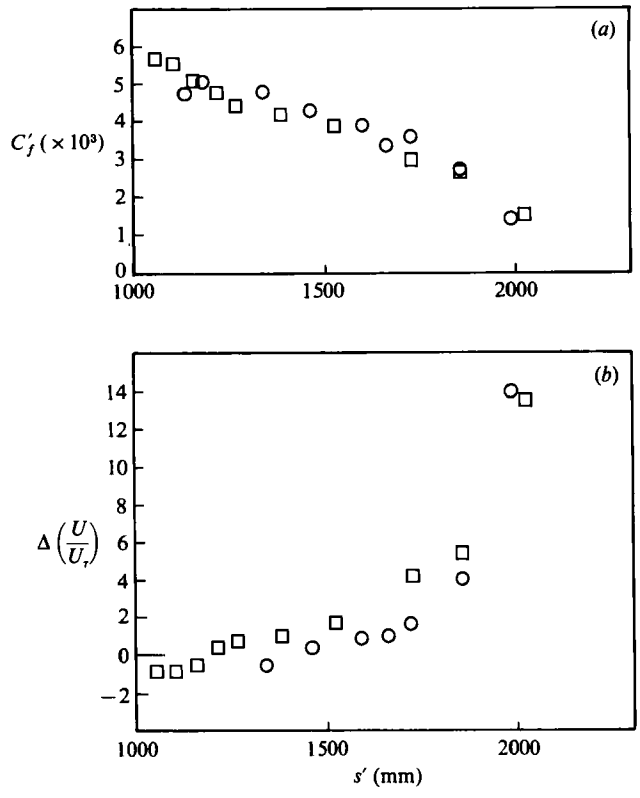

FIGURE 20. Comparison of (*a*) skin-friction coefficient and (*b*) wake factor: ○, curved hill; □, free wing (corrected for effective origin).

thickness of the logarithmic region in the hill flow, are shown in figure 17*b*, and the behaviour of δ_i and δ_c in the two layers is approximately the same.

The integral parameters for the internal layer (denoted by the subscript i) were evaluated by integrating the profiles up to the point where $n = \delta_i$. These values agree well with the results for the wing flow (figure 19). The almost identical growth of momentum thickness, which is normally used to determine the origin of a boundary layer, indicates that the correction for the effective origin is of the right sense and size. The skin-friction and wake-factor distributions shown in figure 20 for the two flows are now consistent with each other (the higher the skin friction, lower the wake factor), even though the correction for the effective origin makes the agreement in the skin-friction distributions slightly worse. However, the differences in C_f introduced by the correction for the effective origin can be accounted for if either δ_i or δ_c is used instead of δ in defining the curvature parameter; both δ_i/R and δ_c/R for the hill flow are smaller than in the free-wing flow. The modified curvature parameter ranges from approximately 0.004 to 0.016, and it can be seen that the internal layer suffers only mildly from the effects of curvature, and the effects of streamwise pressure gradients are likely to dominate.

The momentum-thickness Reynolds numbers and the pressure-gradient parameter in the two flows (figure 19*d*,*e*), as well as the consistent variation of the wake factor with δ_c/R suggests that a general relation such as $C_f = f(R_\theta, \Delta(U/U_\tau), \beta_i, \delta_c/R)$ exists.

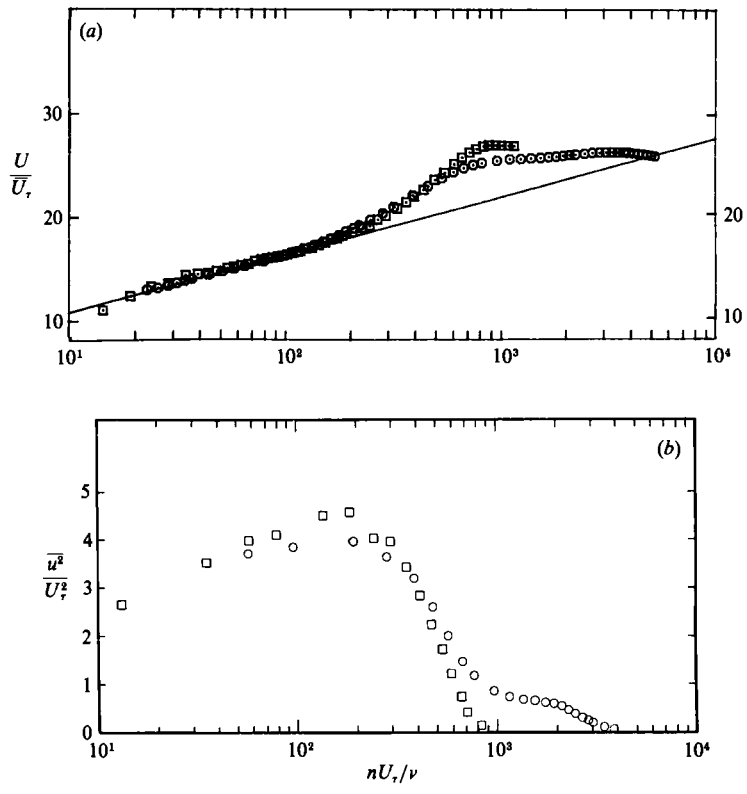

FIGURE 21. Profiles at $s' = 1862$ mm ($C_f = 0.002684$). (*a*) Mean velocity; (*b*) longitudinal turbulent intensity: ○, curved hill; □, free wing.

This view is supported by the results shown in figure 21, where profiles of U and $\overline{u^2}$ at $s' = 1862$ mm are compared. At this location, the values of C_f are equal. The profiles are virtually identical up to the point of maximum deviation in U/U_τ, a fact consistent with the suggested functional form since the variables on the right-hand side are also equal. At this location, the internal and free-wing boundary layers appear to be 'completely' similar and independent of initial conditions. The suggested functional relationship implies that for a given C_f, β_i, and δ_c/R, the wake factors at two widely different R_θ cannot be the same. Also, the internal layer appears to behave as an independent boundary layer with a logarithmic or wall region and a wake region (i.e. region between the edge of the logarithmic region and δ_c). Since the mean velocity variations beyond δ_c do not appear to contribute to the skin friction, this part of the profile behaves as an isolated external layer.

Further evidence for the existence of an internal boundary layer surrounded by an external turbulent field comes from an inspection of the flatness factors, $F_u(=\overline{u^4}/(\overline{u^2})^2)$, $F_v(=\overline{v^4}/(\overline{v^2})^2)$, and $F_w(=\overline{w^4}/(\overline{w^2})^2)$, shown in figure 22. Flatness factors are related to intermittency, a property often used to study interacting shear layers (Dean & Bradshaw 1976; Andreopoulos & Bradshaw 1980). The distributions of the flatness factors over the front flat plate are representative of fully developed turbulent boundary layers, showing near Gaussian values in the inner half of the layer. For a Gaussian on–off process, the flatness factor is given by 3/(intermittency factor). In fully developed turbulent shear layers, this relationship describes the

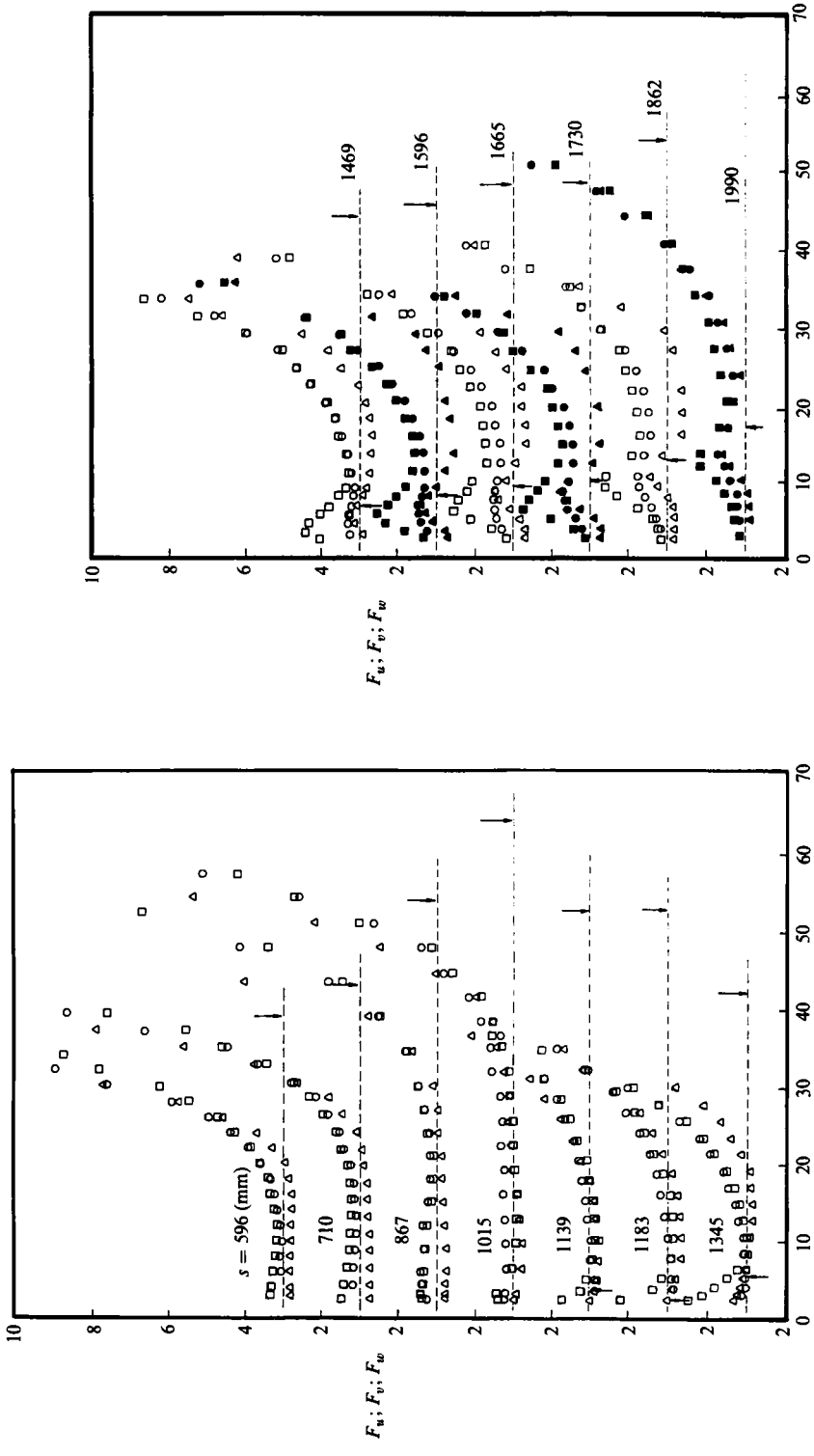

FIGURE 22. Profiles of flatness factors for curved hill. △, $F_u(=\overline{u^4}/(\overline{u^2})^2$; □, $F_v(=\overline{v^4}/(\overline{v^2})^2$; ○, $F_w(=\overline{w^4}/(\overline{v^2})^2$. ———, Gaussian; ↑$\delta_i$; ↓$\delta$. (Solid symbols in the right half of figure for clarity of distributions at alternate stations.) Note shift in the ordinate scale.

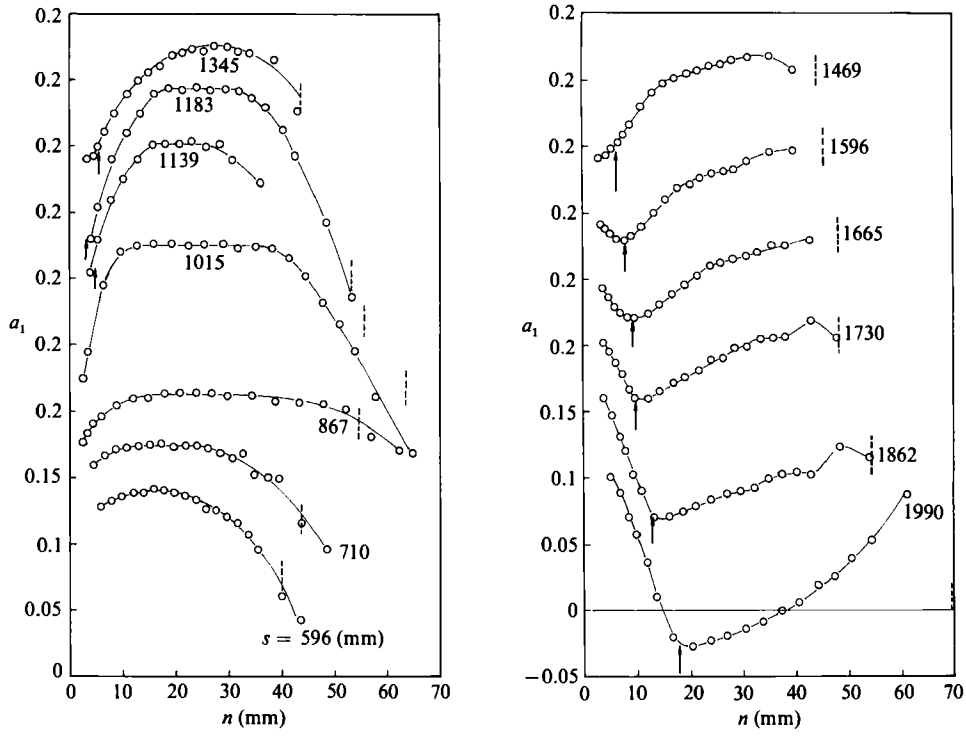

FIGURE 23. Profiles of structural parameter, $a_1(=-\overline{uv}/\overline{q^2})$. $\uparrow \delta_1$; $\dagger \delta$. Note shift in ordinate scale.

flatness-factor distribution over most of the shear-layer thickness (Wood & Bradshaw 1982; Muck *et al.* 1985), and it is useful in a qualitative discussion of flatness-factor distributions. The extent of the near-Gaussian region extends further outward from the wall near the foot of the hill and in the concave bend. In this region the flow is yawed, and the behaviour is similar to that reported by Bradshaw & Pontikos (1985) in a three-dimensional turbulent boundary layer. The extent of this near-Gaussian region decreases significantly at the exit, and there is a large increase in F_v (a decrease in the intermittency) close to the wall. This increase in F_v indicates that turbulence is relatively less intense, and that the flow in the internal layer is tending to depart from the fully turbulent state. However, further downstream over the convex surface, F_v near the wall recovers to a value close to 3, indicating a return to the fully turbulent state. The internal layer at the exit region appears to be in a transitional state, and the low shear-stress levels measured close to the wall in the exit region are consistent with this view. A similar increase in F_v was indirectly detected as a decrease in intermittency by others in strongly accelerated flows (Simpson 1979; Blackwelder & Kovasznay 1972). Furthermore, the constant skin-friction value of 0.005 proposed by Narasimha & Sreenivasan (1973) for the reverse transitional state agrees well with the values observed at the exit region (s = 1139 and 1183 mm). However, the internal layer after this transitional state does not reach a quasi-laminar state as reported by these authors, and the law of the wall reappears near the wall in its usual form at the very next station. Since F_v near the wall recovers much more slowly, the internal layer appears to be in an underdeveloped, turbulent state. The presence of the logarithmic law alone in any flow does not necessarily signify that the flow is fully

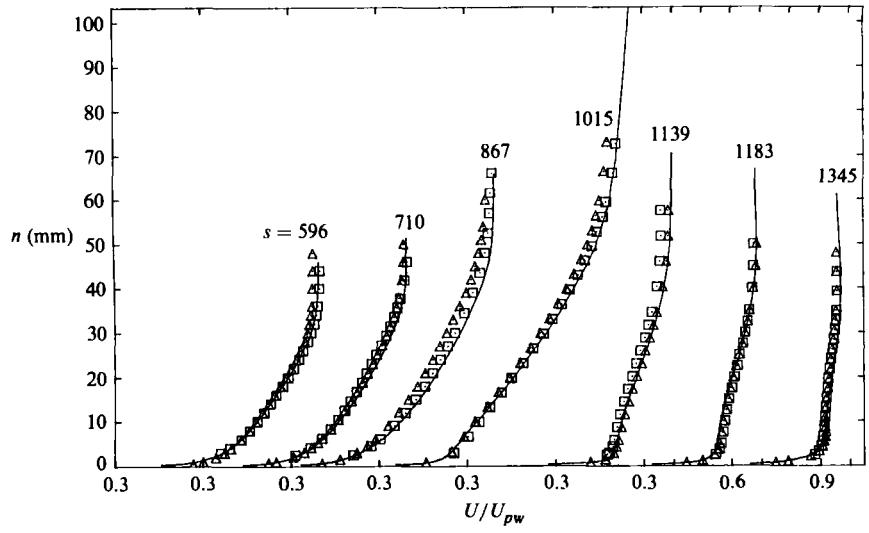

FIGURE 24. Mean velocity profiles around the concave bend. ——, Pitot tube; △, normal wire; □, crossed wire (*UV*-Mode). Note shift in abscissa scale.

turbulent. The slow recovery of F_v also resembles the recovery from the effect of tripping devices as discussed by Coles (1962).

Downstream, all the flatness factors increase to a distinct peak value, located at a distance slightly smaller than δ_i and close to δ_c. This peak is not typical of flows suffering pressure gradients. Simpson, Chew & Shivaprasad (1981) concluded that pressure gradients do not alter the flatness-factor distributions significantly. Beyond this peak, the flatness factors decrease to a minimum before increasing steeply towards the local free stream. This unusual behaviour of the flatness factors, especially the formation of the peak close to δ_c, indicates that there are two distinct interacting turbulent zones. The distributions below the peak, when compared to the distributions in unperturbed boundary layers, show that in this respect the internal layer in the hill flow behaves as an independent boundary layer. The distribution of the flatness factors beyond the peak corresponds to the behaviour expected in a free external turbulent zone.

The turbulent structure of the flow over the hill may be discussed using the parameter a_1, the ratio of shear stress $-\overline{uv}$ to the total turbulent kinetic energy $\overline{q^2}(=\overline{u^2}+\overline{v^2}+\overline{w^2})$ (see figure 23). The distributions at the first two stations are typical of 'simple' shear layers, with a near-constant value of approximately 0.14. The slight reduction near the foot of the hill is due to the yawing of mean streamlines (Bradshaw & Pontikos 1985). The large increase in the bend is due to concave curvature, and it persists over the exit region. Further downstream over the convex surface, a_1 decreases across the internal layer and increases across the external layer, with a minimum at $n = \delta_i$.

This uneven distribution of a_1, especially the formation of a minimum, does not appear to be due to the pressure gradients, since Tsuji & Morikawa (1976) report a constant distribution of a_1 across the boundary layer, ranging from 0.11 to 0.16, in their flat-plate flow. The minimum appears instead to be due to the interaction between the internal and external layers. The inflexion in the mean velocity profiles

is plotted in the physical coordinate system around the concave bend in figure 24, and the sense of the mean shear above the internal layer during its initial developmental stage supports the earlier suggestion that the external layer behaves as a free mixing layer. Direct numerical simulations of the complete time-dependent Navier–Stokes equations, (Spalart & Leonard 1985) show that a change in species of the large-scale structure occurs whenever there is an inflexional instability in the mean velocity profile. A similar change in species of large-scale structures in the present flow could explain the abnormal behaviour of normal stresses at the exit region. Since the mean streamlines converge towards the wall as the flow accelerates near the exit, the eddying motions in the external layer are affected by the wall constraint, $v = 0$, which sets up pressure fluctuations so that the energy is distributed among the normal stress components (see §3.2). The subsequent streamwise decrease of the structural parameter in the external layer is only gradual, unlike that found in other strongly curved flows (Gillis & Johnston 1983; So & Mellor 1972; Prabhu & Sundarasiva Rao 1981).

4. On the perturbation in the hill flow and implications for the effects of convex curvature

Thus far, it has been shown that an internal boundary layer forms over the convex region of the hill. However, the perturbation responsible for its growth is yet to be identified. Internal layers grow whenever there is a mismatch between the shear stress in the vicinity of the wall and the wall shear stress inferred from the law of the wall. A large mismatch first occurs at the exit region, where the internal boundary layer originates. One perturbation that could produce such a mismatch is the change in pressure gradient, which changes the velocity and the Reynolds-stress components in the inner region, while leaving these quantities largely unaffected in the outer region. However, since the internal-flow behaviour near its origin is not consistent with that produced by a pressure gradient, it does not appear to be the primary mechanism. The abrupt change in surface curvature at the exit region suggests an alternative triggering mechanism, and this is verified below.

In many strongly curved flows with diverse external conditions (So & Mellor 1972; Smits *et al.* 1979*a*,*b*; Gillis & Johnston 1983; Prabhu & Sundarasiva Rao 1981), a similar mismatch was found at the beginning of the curved section, with the subsequent appearance of an internal layer. In most of these flows, the mismatch could well be caused by the favourable pressure gradient that usually occurred at the junction between the flat and the curved surfaces. In the experiment by Gillis & Johnston (1983), however, the streamwise pressure gradient was kept near zero everywhere, and yet the mismatch still appeared at the beginning of the curved section (refer to figure 12 in Gillis & Johnston 1983). Hence, a sudden change in surface-curvature change can provide the required perturbation. To check this, we have plotted the total pressure against the stream function for the flow of Gillis & Johnston (1983) in figure 25. The thickness of the internal layer inferred from this plot (13.8 mm) agrees reasonably well with that inferred from the extrapolation of data points below the knee in their shear-stress profile (11.6 mm). The total pressure–stream function plot for the hill flow (figure 18) shares a similar feature with that of figure 25 in that the total pressure does not change till the curved wall turns through a certain angle. For the Gillis & Johnston experiment, the change in total pressure first occurs at 30°, while in the present case the changes were first noticed after approximately 13° of convex curvature. The Reynolds stresses in the vicinity

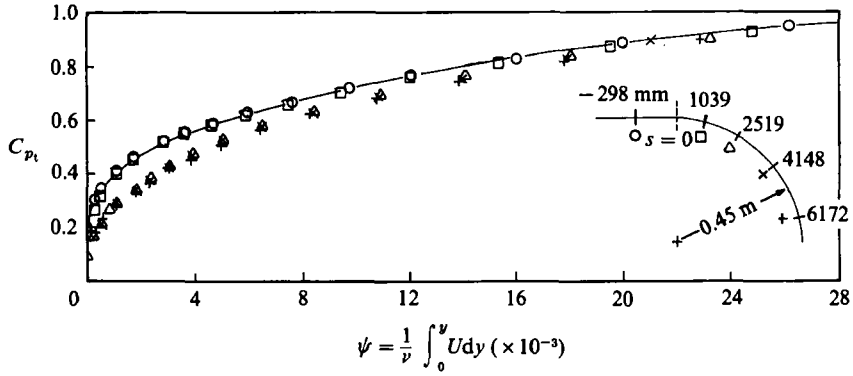

FIGURE 25. Total pressure versus stream function plot for the strongly curved zero-pressure-gradient flow of Gillis & Johnston (1983).

of the wall, however, change as soon as the step change in surface curvature occurs in both cases (see for example figure 2 of Gillis & Johnston 1983). This lag in the change in total pressure behind that of the Reynolds stresses also shows that the pressure gradient is not the primary cause of the evolution of the internal boundary layer in the hill flow.

In the contrast to these results, the results of Gibson, Verriopoulos & Vlachos (1984) do not exhibit any mismatch (refer to their figure 7) and knee points are not seen in their turbulence profiles. However, the step change in surface change in surface curvature is much weaker ($\Delta k = (1/R_2 - 1/R_1) = 0.41$ m^{-1} for Gibson *et al.*, and $\Delta k = 2.2$ m^{-1} for Gillis & Johnston).

The absence of the mismatch in mildly curved flows implies that a threshold in Δk is necessary to initiate an internal-layer growth. By dimensional analysis,

$$\delta_1 = f(u_{\tau_0}, \nu, \Delta k, s''), \tag{1}$$

where the suffix 0 indicates the conditions upstream of the step and s'' is the downstream distance from the step. Hence,

$$\frac{\delta_1 U_{\tau_0}}{\nu} = f\left(\frac{\Delta k \nu}{U_{\tau_0}}, \frac{s'' U_{\tau_0}}{\nu}\right). \tag{2}$$

The parameter $\Delta k^* = \Delta k \nu / U_{\tau_0}$ represents the strength of the perturbation due to the sudden change in surface curvature, and it will be referred to as the 'wall-curvature perturbation parameter'. For a given $s'' U_{\tau_0}/\nu$, $\delta_1 U_{\tau_0}/\nu$ is non-zero if an internal layer is present due to a mismatch. Values of Δk^* derived from previous experiments on convex wall flows are listed in table 1. The data fall into two groups: mild curvature (where 0.065×10^{-4} is the highest value) and strong curvature (where 0.373×10^{-4} is the lowest value). The threshold should obviously lie between these limits. The values of Δk^* near the exit region of the hill flow (0.516×10^{-4} if U_{τ_0} in the concave bend is used and 0.676×10^{-4} if U_{τ_0} at the first measuring station is used) are approximately the same as in the other strongly curved flows. In addition, since the mismatch and the changes in total pressure and Reynolds stresses close to the wall are the same as that in the zero-pressure-gradient flow of Gillis & Johnston (1983), the internal boundary layer must be triggered by the abrupt change in surface curvature.

The perturbation due to a step change in curvature has some interesting implications for the effects of convex curvature in general. Apparently, the effects of the

Authors	$\Delta kv/U_{\tau_0} \times 10^4$
Gibson *et al.* (1984)	0.064
Muck *et al.* (1985)	0.041
Ramaprian & Shivaprasad (1978)	0.065
So & Mellor (1972)	0.620
Gillis & Johnston (1983)	0.545 (1st expt)
	0.553 (2nd expt)
	0.526 (3rd expt)
Prabhu *et al.* (1983)	0.385 (case A1)
	0.373 (case B1)
	0.474 (case C1)
Present case	0.516 (U_{τ_0} at Concave Bend)
	0.676 (U_{τ_0} at 1st station)

TABLE 1. Wall curvature perturbation parameter, $\Delta kv/U_{\tau_0}$ in convex-wall boundary-layer experiments

curvature-perturbation parameter Δk^* and the curvature parameter δ/R are different and need to be distinguished. The effect of the former is felt close to the wall as soon as the curved surface begins, while the latter affects the flow significantly only far from the wall. All the available turbulence results in curved flows show that the changes in the outer flow occur only after the flow has turned through a certain turning angle. In a flow with a mild change in curvature, the effects of Δk^* are negligible so that the flow does not initially undergo much structural change close to the wall. Prolonged mild streamline curvature eventually affects the structure in the outer portions of the flow to a degree that depends on the magnitude of the curvature parameter. In the mildly curved flows listed in table 1, structural changes occur only above $n/\delta > 0.8$. In contrast, in a flow with a strong change in surface curvature, the effect of Δk^* is significant and it is felt very quickly in the vicinity of the wall. Structural changes follow immediately after the step change, and an internal layer forms, which isolates the flow above it (Gillis & Johnston 1983). Friction-dependent and friction-independent regions are formed (Prabhu, Narasimha & Rao 1983), regardless of the upstream-boundary-layer thickness. Therefore, the conventional curvature parameter δ/R fails to describe the flow behaviour, and the appropriate parameter is δ_i/R or δ_c/R. Since the thickness of the internal layer is small in comparison with the radius of curvature, the skin-friction distribution over a strongly curved wall actually reflects the effects of prolonged mild curvature. The internal boundary layer does not grow all that rapidly, provided external conditions such as pressure gradient and local wall curvature do not change; hence, the total pressure, Reynolds stresses and skin-friction coefficients are unlikely to change quickly. This results in the apparently asymptotic or saturated behaviour reported in all strongly curved flows.

5. Remarks on the studies of wind flow over hills in relation to the present hill flow

Meteorological studies of wind flow over hills usually examine changes in the wind speed and the turbulence due to changes in surface elevation. The upwind boundary layer generally corresponds to a neutrally stable atmosphere, the ratio of the thickness of the reference boundary layer to the maximum elevation is large ($\delta/h \gg 1$),

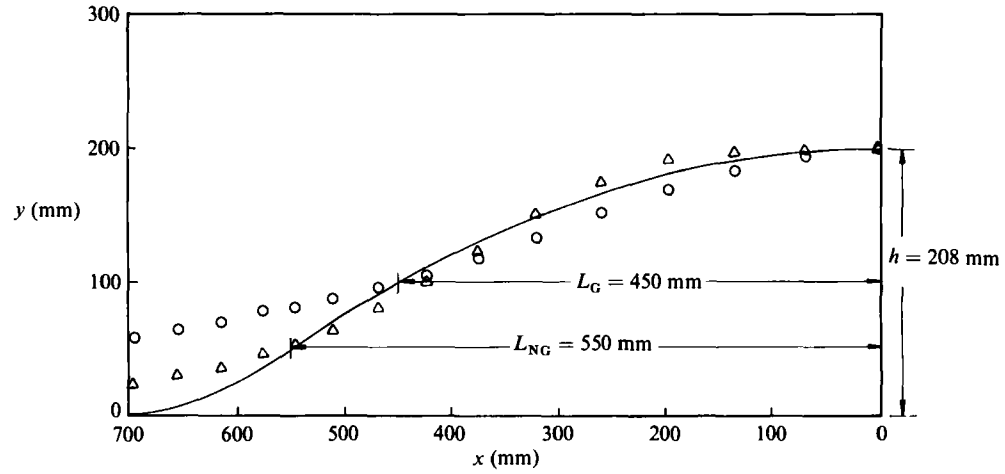

FIGURE 26. Profile shape and lengthscales for the curved hill: ——, actual profile; ○, Gaussian approximation, $f(x/L) = 1/[1+(x/L_G)^2]$; △, non-Gaussian approximation, $f(x/L) = 1/[1+3(x/L_{NG})^4]$.

and the terrain conditions are simulated by means of properly scaled rough surfaces (for example, see Britter *et al.* 1981 for a discussion). In the present hill flow, since the aim of the study is to understand the effects of streamline curvature, these scaling laws were not considered. For instance, the ratio of the boundary-layer thickness on the leading-edge plate to the height of the hill in the present experiment is only 0.4, and the surface is smooth everywhere. The results of the present study should therefore be treated with caution, if they are to be compared to those obtained in either a properly simulated model experiment or field results, and 'scale effects' are likely to play a major role. However, a qualitative comparison is possible, and for this purpose we have used the theory of Jackson & Hunt (1975).

Jackson & Hunt divided the flow into two regions, namely an inner constant-stress region (logarithmic region) and an outer region. By expressing the changes in the wind speed as a perturbation to the upwind value, solutions were presented for the inner and outer regions using the linearized small-perturbation form of the mean momentum equations. Perturbations in the shear-stress field were derived by using the eddy-viscosity hypothesis to obtain closure. The mean velocity distribution at a reference location over the level ground was expressed in the form

$$U_0(y) = \frac{U_{\tau_0}}{\kappa} \ln \frac{y}{y_0} \quad \text{for } y < \delta, \tag{3}$$

$$U_0(y) = \frac{U_{\tau_0}}{\kappa} \ln \frac{\delta}{y_0} \quad \text{for } y > \delta, \tag{4}$$

Suffix 0 denotes reference quantities in the upwind flows and κ, y_0 and y are the Kármán constant (= 0.41), roughness length and distance normal to the level ground respectively. Using the mean velocity profile at the first measuring station in the present hill flow as the reference gives $U_{\tau_0} = 0.76$ m/s and $y_0 = 2.35 \times 10^{-6}$ m. It should be noted here that the inner logarithmic region in our reference boundary layer does not extend to the boundary-layer edge, unlike that specified by (3). The shape of the curved hill can be expressed to a good approximation as $y = h\{1/1+3(x/L)^4\}$.

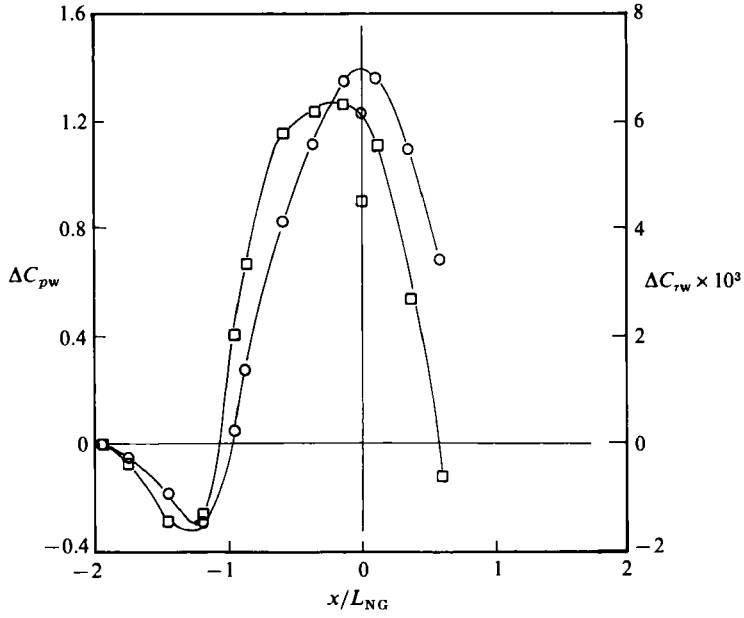

FIGURE 27. Streamwise surface pressure and shear-stress perturbations with respect to reference upwind values at $x/L_{NG} = -2$. ○, ΔC_{pw}; □, $\Delta C_{\tau w}$.

The actual profile is compared with this approximation and that for the Gaussian hill considered by Jackson & Hunt in figure 26. The horizontal lengthscales corresponding to both non-Gaussian ($L_{NG} = \frac{1}{4}h$) and Gaussian ($L_G = \frac{1}{2}h$) distributions are 0.55 m and 0.45 m respectively.

The analysis is based on small-perturbation theory and requires $h \ll L$ such that the perturbation velocities are very small ($\epsilon \ll 1$). The values for h/L, the thickness of the inner region, and ϵ in the present hill flow are 0.36, 20 mm and 15 respectively. Therefore the theory is not quantitatively valid in the present case. However, Jackson & Hunt reported that the theory was capable of qualitatively describing any hill flow in terms of the perturbation variables (pressure, velocity and shear stress), even when the upwind-profile thickness was smaller than the height of the hill.

To facilitate these qualitative comparisons, the changes in the non-dimensional wall static pressure $\Delta C_{pw} (= C_{pw} - C_{pw0})$ and the non-dimensional surface shear stress, $\Delta C_{\tau_\omega} (= C_{\tau_\omega} - C_{\tau_{\omega 0}})$ for the current experiment are plotted in figure 27. The change in surface shear stress occurs before the change in static pressure, and ΔC_{τ_ω} reaches a maximum just ahead of the crest, as predicted by the theory. The fractional change in the mean velocity above the hill crest is shown in figure 28. This ratio is referred to as the 'fractional speed-up ratio' and denoted as ΔS in meteorological terminology. The shape of the profile, especially the occurrence of a maximum in ΔS at a small distance above the hill surface, is in qualitative agreement with the theory. According to the analysis, the internal-layer thickness is given by the height of the maximum velocity perturbation. In the present hill flow, however, the maximum velocity perturbation occurs well inside the present internal layer.

Another interesting feature in wind flow over hills is the development of sharp mean velocity gradients near the surface at the crest associated with the formation of a local maximum in the mean velocity profiles. This maximum has been given the name

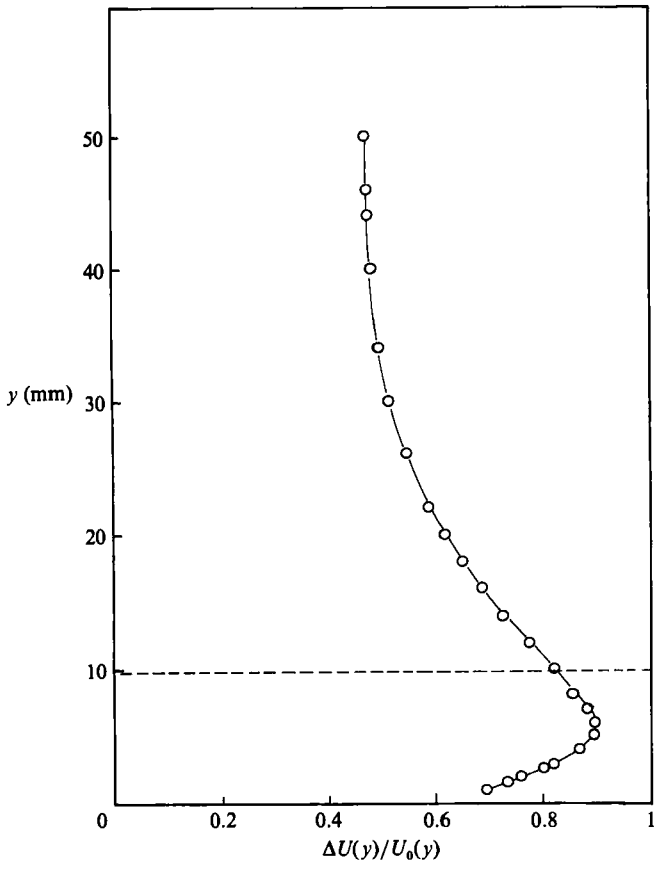

FIGURE 28. Profile of 'fractional speed-up ratio' over the hill at $x/L_{NG} = 0$; ----, $y = \delta_1$.

'jet' in meteorology. In the present hill flow such a feature is present at the exit region (figure 24).

The fractional changes in Reynolds stresses are shown in figure 29. All the perturbation stresses are positive close to the surface and change sign more or less at a height where ΔS is a maximum. According to the theory, the whole flow is dominated by the changes that occur within the internal layer. In addition, the perturbation shear stress should be at its maximum close to the surface and fall gradually to zero at the edge of the inner region. This feature is qualitatively reproduced in the present results, and again the pressure-gradient-perturbed inner region does not extend to the edge of the internal boundary layer. The decrease in all the stress components is consistent with the effect of prolonged convex curvature at the edge of the present internal layer.

Beyond the inner region, the changes in the turbulence in wind flows over hills have been described using rapid-distortion theory (Britter *et al.* 1981) and found to be in agreement with experiments. For symmetric hills like the present one, rapid-distortion theory predicts an increase in $\overline{v^2}$ and a decrease in $\overline{u^2}$, while in the present case all the perturbation-stress components decrease and reach a minimum at the edge of the internal boundary layer. Therefore, the behaviour of turbulence above the inner region in the present experiment is considerably different from that

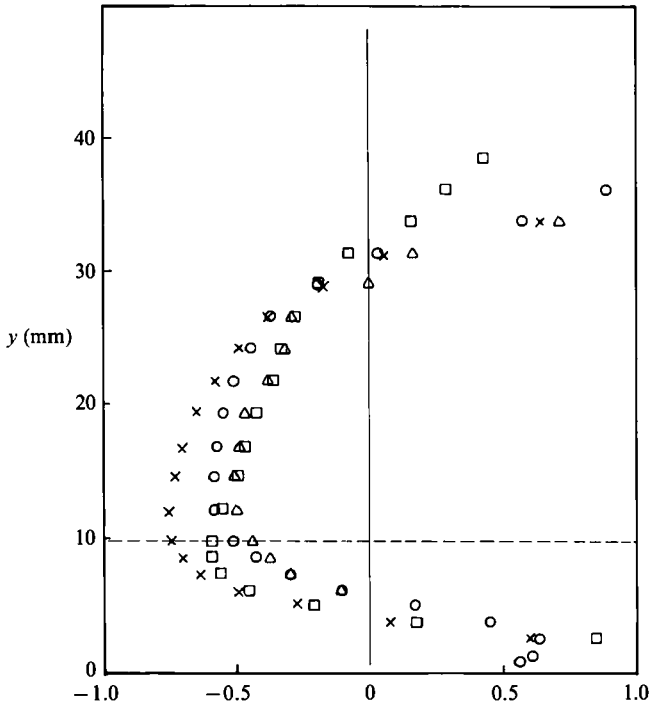

FIGURE 29. Profiles of perturbation Reynolds stresses over the hill at $x/L_{NG} = 0$. ○, $\Delta\overline{u^2}/\overline{u_0^2}$; □, $\Delta\overline{v^2}/\overline{v_0^2}$; △, $\Delta\overline{w^2}/\overline{w_0^2}$; ×, $\Delta(-\overline{uv})/(-\overline{uv})_0$; ----, $y = \delta_i$.

observed in hill-flow studies. The apparent reason for this difference is the effect of prolonged convex streamline curvature, as all the stress components consistently decrease. In contrast, the curvature effect was found to be negligible for the slender Gaussian hill considered by Jackson & Hunt (1975).

6. Conclusions

The results from the experiments on a biconvex 'free wing' and a two-dimensional 'curved hill' show that an internal boundary layer grows over the hill. Its behaviour is similar to that of the boundary layer growing over the free wing. The flatness-factor distributions, together with the behaviour of the structural parameter a_1, show that the internal boundary layer is shrouded by an external free turbulent flow. The behaviour of the external flow is in qualitative agreement with that reported in free turbulent flows affected by a wall constraint. Apparently, a bifurcation occurs in the initial boundary-layer structure ahead of the convex region and the internal and external layers behave almost completely independently.

The internal layer forms in a region where the flow experiences a reverse transitional state, without undergoing relaminarization, followed by a recovery to a fully developed turbulent state. After the recovery of the logarithmic region and the flatness factor further downstream, the flow in the inner region of the internal layer is mainly affected by the changes in pressure gradient, while the prolonged mild streamline curvature affects the outer or wake region of the internal layer, in addition to the effects induced by the external free turbulent flow. The ratio of the

internal-layer thickness to the surface radius of curvature appears to represent the effects of prolonged convex curvature more accurately than the conventional ratio based on the overall thickness. The internal layer appears to determine the skin-friction distribution and the process of separation independently of the presence of the external layer.

The initial transitional state of the internal layer, and the fact that the streamwise total pressure change lags behind the changes in the Reynolds stresses near the origin of the internal layer show that the pressure gradient is not the primary perturbation mechanism responsible for initiating the internal-layer growth. It appears, in fact, that it is the abrupt change in surface curvature (concave to convex) that triggers the internal-layer growth.

Dimensional analysis shows that the perturbation due to a step change in surface curvature could be represented by a 'wall-curvature-perturbation parameter', Δk^*. The absence of internal layers in the mildly curved flows suggests that a threshold in Δk^* must be exceeded before internal layers are formed. The available data suggest a lower limit for the threshold value of 0.373×10^{-4}.

The effect of the wall-curvature-perturbation parameter Δk^* is different from the effect of the curvature parameter δ/R. The wall-curvature-perturbation parameter describes the flow close to the surface immediately following the change, while the curvature parameter describes the behaviour in the region further away from the wall. The changes due to the effect of the curvature parameter begin only after the flow turns through some angle. High levels of Δk^* affect the structure in the vicinity of the step, and result in the growth of an internal layer. Since it is this internal layer that determines the skin friction, and since its thickness is relatively small compared to the radius of curvature, the prolonged streamline curvature has only a mild effect on the subsequent flow behaviour. In contrast, in a mildly curved flow with a small Δk^* the effect of the step change in wall curvature is negligible and the flow does not exhibit any significant changes in the structure near the step. This is probably why a mildly curved flow behaves differently from a strongly curved flow. Once formed, the internal layer determines the skin-friction distribution, and a saturated behaviour results, as observed in all strongly curved flows.

A qualitative comparison with meteorological studies of the flow over hills shows that the internal layer in the present case is thicker than the pressure-gradient-perturbed inner region described in meteorological flows. However, the changes within this inner region are consistent with those reported in both experimental studies and the theory of Jackson & Hunt (1975) for wind flow over hills. The changes above this inner region in the present case are not consistent with those predicted by the rapid-distortion analysis, unlike the case in meteorological flows. However, any comparison should be performed with care since the scaling laws describing the dynamic similitude of natural wind flows are not obeyed in the present experiments.

The authors are deeply indebted to Professor P. Bradshaw for his constructive comments during the preparation and revision of the manuscript. This project was financially supported by the Australian Research Grants Scheme. One of us (A.J.S.) received additional support from AFOSR Grant 85-0126, monitored by Dr James McMichael.

REFERENCES

ABELL, C. J. 1977 Scaling laws for pipe flows. Ph.D. thesis, University of Melbourne.

ANDREOPOULOS, J. & BRADSHAW, P. 1980 *J. Fluid Mech.* **100**, 639.

ANDREOPOULOS, J. & WOOD, D. H. 1982 *J. Fluid Mech.* **118**, 143.

BASKARAN, V. 1983 Turbulent flow over a curved hill. Ph.D. thesis, University of Melbourne.

BASKARAN, V. & JOUBERT, P. N. 1984 Mean and turbulent flow data for a boundary layer over a two-dimensional curved hill. Rep. FM-16. Department of Mech. Eng., University of Melbourne.

BLACKWELDER, R. F. & KOVASZNAY, L. S. G. 1972 *J. Fluid Mech.* **53**, 61.

BRADLEY, E. F. 1980 *Q. J. R. Met. Soc.* **106**, 101.

BRADSHAW, P. 1973 Effects of streamline curvature on turbulent flow. *AGARDograph* 169.

BRADSHAW, P. & PONTIKOS, N. S. 1985 *J. Fluid Mech.* **159**, 105.

BRADSHAW, P. & UNSWORTH, K. 1974 An improved FORTRAN program for Bradshaw–Ferris–Atwell method of calculating turbulent shear layers. *I.C. Aero Rep.* 74–02.

BRITTER, R. E., HUNT, J. C. R. & RICHARDS, K. J. 1981 *Q. J. R. Met. Soc.* **107**, 91.

CASTRO, I. P. & BRADSHAW, P. 1976 *J. Fluid Mech.* **73**, 265.

CHANDRSUDA, C. & BRADSHAW, P. 1981 *J. Fluid Mech.* **110**, 171.

COLES, D. E. 1962 The turbulent boundary layer in a compressible fluid. *Rep.* R-403-PR. Rand Corp., Santa Monica.

DE BREDERODE, V. & BRADSHAW, P. 1974 A note on the empirical constants appearing in the logarithmic law for turbulent wall flows. *I.C. Aero Rep.* 74–03.

DEAN, R. B. & BRADSHAW, P. 1976 *J. Fluid Mech.* **78**, 641.

DUMAS, R. & FULACHIER, L. (eds) 1982 *Proc. IUTAM Symp. Structure of Complex Turbulent Shear Flows, Marseille.*

GIBSON, M. M., VERRIOPOULOS, C. A. & VLACHOS, N. S. 1984 *Exp. Fluids* **2**, 17.

GILLIS, J. C. & JOHNSTON, J. P. 1983 *J. Fluid Mech.* **135**, 123.

HALL, P. 1984 The Görtler vortex instability mechanism in three-dimensional boundary layers. *NASA CR*-172370.

HOFFMANN, P. H., MUCK, K. C. & BRADSHAW, P. 1985 *J. Fluid Mech.* **161**, 371.

JACKSON, P. S. & HUNT, J. C. R. 1975 *Q. J. R. Met. Soc.* **101**, 929.

JONES, W. P. & LAUNDER, B. E. 1972 *J. Fluid Mech.* **56**, 337.

KLINE, S. J., CANTWELL, B. J. & LILLEY, G. M. (ed) 1982 *Proc. 1980–81 AFOSR–HTTM Stanford Conf. on Complex Turbulent Flow*, Vol. 1. Thermosciences Div., Stanford University.

MARUMO, E., SUZUKI, K. & SATO, T. 1978 *J. Fluid Mech.* **87**, 121.

MUCK, K. C. 1982 Turbulent boundary layers on mildly curved surfaces. Ph.D. thesis, Imperial College, London.

MUCK, K. C., HOFFMANN, P. H. & BRADSHAW, P. 1985 *J. Fluid Mech.* **161**, 347.

NARASIMHA, R. & SREENIVASAN, K. R. 1973 *J. Fluid Mech.* **61**, 417.

PATEL, V. C. 1965 *J. Fluid Mech.* **23**, 185.

PERRY, A. E. 1982 *Hot-Wire Anemometry.* Clarendon.

PRABHU, A., NARASIMHA, R. & RAO, B. N. S. 1982 Structure and mean flow similarity in curved turbulent boundary layers. In *Proc. IUTAM Symp. Structure of Complex Turbulent Shear Flows, Marseille* (ed. R. Dumas & L. Fulachier)

PRABHU, A. & SUNDARASIVA RAO, B. N. 1981 Turbulent boundary layers in a longitudinally curved stream. *Rep.* 81 FM 10. I.I.Sc., Bangalore, India.

PURTELL, L. P., KLEBANOFF, P. S. & BUCKLEY, F. T. 1981 *Phys. Fluids* **24**, 802.

RAMAPRIAN, B. R. & SHIVAPRASAD, B. G. 1978 *J. Fluid Mech.* **85**, 273.

SIMPSON, R. L. 1979 Some features of strongly accelerated boundary layers. In *Second Symp. on Turbulent Shear Flows, Imperial College, London.*

SIMPSON, R. L., CHEW, Y. T. & SHIVAPRASAD, B. G. 1981 *J. Fluid Mech.* **113**, 53.

SMITS, A. J., EATON, J. A. & BRADSHAW, P. 1979*a* *J. Fluid Mech.* **94**, 243.

SMITS, A. J., MATHESON, N. & JOUBERT, P. N. 1983 *J. Ship Res.* **27**, 147.

SMITS, A. J. & WOOD, D. H. 1985 *Ann. Rev. Fluid Mech.* **17**, 321.

SMITS, A. J., YOUNG, S. T. B. & BRADSHAW, P. 1979*b* *J. Fluid Mech.* **94**, 209.

SO, R. M. C. & MELLOR, G. L. 1972 An experimental investigation of turbulent boundary layers along curved surfaces. *NASA CR*-1940.

SPALART, P. R. & LEONARD, A. 1985 Direct numerical simulation of equilibrium turbulent boundary layers. In *Fifth Symp. on Turbulent Shear Flows, Cornell University, Ithaca, New York.*

TANI, I. 1968 In *Proc. AFOSR–IFP–Stanford Conf. on Computation of Turbulent Boundary Layers* (ed. S. J. Kline, M. V. Morkovin, G. Sovran & D. J. Cockrell), pp. 483–494. Thermosciences Div., Dept. of Mechanical Engineering, Stanford University.

TAYLOR, P. A. 1977 *Boundary-Layer Met.* **11**, 439.

TSUJI, Y. & MORIKAWA, Y. 1976 *Aero. Q.* **27**, 15.

WOOD, D. H. & BRADSHAW, P. 1982 *J. Fluid Mech.* **122**, 57.

WOOD, D. H. & BRADSHAW, P. 1984 *J. Fluid Mech.* **139**, 347.